

VLADIMIR I. KONDRATIEV

Processing and characterization of  
transparent electrode materials





**VLADIMIR I. KONDRATIEV**

Processing and characterization of  
transparent electrode materials



UNIVERSITY OF TARTU  
Press

The study was carried out in Department of Materials Science, Institute of Physics, Faculty of Science and Technology, University of Tartu, Estonia

The Dissertation was admitted on June 15, 2017 in partial fulfilment of the requirements for the degree of Doctor of Philosophy in Materials Science and allowed for defence by Scientific Council on Materials Science of the Faculty of Science and Technology, University of Tartu.

Supervisors: Prof. Dr. Alexey E. Romanov, ITMO University, St. Petersburg, Russian Federation; Leonid Dolgov, Institute of Physics, University of Tartu, Tartu, Estonia; School of Chemistry, Sun Yat-Sen University, P. R. China

Opponents: Dr. A.V. Nashchekin, Ioffe Physical Technical Institute, RAS, St. Petersburg, Russian Federation

Dr. T. Dedova, Department of Materials and Environmental Technology, Tallinn University of Technology, Tallinn, Estonia

Defence: August 24, 2017 at the University of Tartu, Tartu, Estonia

This thesis was financially supported by European Social Fund's Doctoral Studies and Internationalization Program DoRa, "Low-dimensional structures and their applications" SF0180058s07, "Structure sensitive interaction mechanisms in functional materials at nanoscale" IUT2-25, ERDF (Centre of Excellence "Mesosystems: Theory and Applications", TK114), ETF grant "Processing, characterization, and modeling of nanoparticles-reinforced multiscale composites" 8420, Estonian Nanotechnology Competence Centre (EU29996), ERDF "TRIBOFILM" 3.2.1101.12-0028, "IRGLASS" 3.2.1101.12-0027, "Nano-Com" 3.2.1101.12-0010, NATO SPS project grant NUKR.SFPP984702 and the European Union funded by European Regional Development Fund.



ISSN 2228-0928  
ISBN 978-9949-77-505-7 (print)  
ISBN 978-9949-77-506-4 (pdf)

Copyright: V. I. Kondratiev, 2017

University of Tartu Press  
[www.tyk.ee](http://www.tyk.ee)

# CONTENTS

ABBREVIATIONS .....	7
LIST OF PUBLICATIONS .....	8
AUTHOR'S CONTRIBUTION .....	9
INTRODUCTION .....	10
1. BACKGROUND .....	12
1.1. Traditional and novel materials for transparent electrode applications .....	12
1.2. Electrical properties of transparent conductive oxides .....	14
1.3. Optical properties of transparent conductive oxides .....	17
1.4. Highlights of the particular applications of AZO structures tested in this work .....	18
1.4.1. Possibilities to control the fluorescence of AZO structures ...	18
1.4.2. Use of AZO films in the liquid crystal indicators .....	21
1.5. Preparation methods of transparent conductive oxides .....	23
2. GOALS OF THE RESEARCH.....	26
3. EXPERIMENTAL FACILITIES.....	27
3.1. Synthesis of AZO films by spin-coating method .....	27
3.2. Synthesis of AZO films by electrospinning method .....	28
3.3. Preparation of AZO-gold samples for the resonant control of fluorescence .....	29
3.4. Preparation of AZO films for liquid crystal cells .....	30
3.5. Substrate preparation .....	30
3.6. Equipment used for the characterization of prepared samples .....	30
4. RESULTS AND DISCUSSION .....	32
4.1. Continuous AZO coatings: preparation features, electrical properties and light transmittance .....	32
4.2. AZO coatings made of fibers: preparation and properties .....	42
4.3. Optical performance of AZO films used as a part of layered coatings and liquid crystal indicators .....	49
4.3.1. AZO-gold layer for the resonant control of fluorescence .....	49
4.3.2. Use of AZO electrodes in the liquid crystal cell .....	54
CONCLUSIONS .....	57
SUMMARY IN ESTONIAN .....	59
ACKNOWLEDGEMENTS .....	61
REFERENCES .....	62

PUBLICATIONS .....	69
CURRICULUM VITAE .....	107
ELULOOKIRJELDUS .....	109

## **ABBREVIATIONS**

AFM	Atomic force microscope/microscopy
AZO	Aluminium doped zinc oxide
CVD	Chemical vapor deposition
EDX	Energy dispersive X-ray spectrometer/spectroscopy
FIB	Focused ion beam
FTO	Fluorine doped tin oxide
GIXRD	Grazing Incidence X-ray diffraction
ITO	Indium tin oxide
MBE	Molecular beam epitaxy
NIR	Near-infrared
SEM	Scanning electron microscope
TCF	Transparent conducting film
TCO	Transparent conductive oxide
UV	Ultraviolet
XRD	X-ray diffraction

## LIST OF PUBLICATIONS

The thesis is based on the following papers:

- I. V.I. Kondratiev, I. Kink, A.E. Romanov, LOW TEMPERATURE SOL-GEL TECHNIQUE FOR PROCESSING AL-DOPED ZINC OXIDE FILMS, *Materials Physics and Mechanics* (2013), 17, 38–46.
- II. V.I. Kondratiev, I. Kink, A.E. Romanov, L. Dolgov, TRANSPARENT FILMS FROM ALUMINIUM-DOPED ZINC OXIDE FIBERS PREPARED BY ELECTROSPINNING METHOD, *Materials Physics and Mechanics* (2016), 27, 133–141.
- III. L. Dolgov, V.I. Kondratiev, A. Loot, V. Kiisk, S. Lange, Resonant control of fluorescence from aluminium doped zinc oxide films, *Optical and Quantum Electronics* (2016), 48, 522; (doi:10.1007/s11082-016-0794-5).

List of other publications:

- IV. L. Dolgov, O. Fesenko, V. Kavelin, O. Budnyk, V. Estrela-Llopis, A. Chevychalova, T. Repän, V.I. Kondratiev, S. Mamykin, Gold micro- and nano-particles for surface enhanced vibrational spectroscopy of pyridostigmine bromide, *Vibrational Spectroscopy* (2017), 88, 71–79; (doi:10.1016/j.vibspec.2016.11.005).



## AUTHOR'S CONTRIBUTION

The author of the thesis has done an essential part of the work. At the same time it is a product of collective efforts. At some stages of the investigation specialists in materials science, microelectronics and optics have been also involved in the work. It is justified by the complex character of the tasks related to the preparation, characterization, analysis and modelling of the conductive oxide coatings. Solving of the problems in a team is reflected in the joint authorship of the above-mentioned scientific papers, where the outcome of the work has been collected. The author's contribution to each of those papers is specified below.

I. The author has tested several possible chemical routes for preparation of continuous AZO films and determined optimal conditions for deposition and annealing of the coatings. He assembled the setups for drying and annealing of samples in a controlled environment. All samples have been prepared by the author himself. He has actively participated in their characterization by the methods of optical and electronic microscopy. It is important to note that the author developed a simplified handmade setup for fast estimation of the electrical sheet resistance of the samples. The author has actively participated in discussion of the obtained results and preparation of the paper for publication. He has been indicated as the first author of the related paper.

II. The author has optimized electrospinning conditions needed for the deposition of AZO coatings consisting of the nanofibers. Especially, draw attention to the humidity control during sample preparation. He has actively participated in the characterization of the obtained samples by means of scanning electron microscopy and optical photometry. The author actively took part in the discussion of the obtained results and preparation of the related paper. Due to his major contribution to the paper's concept and its implementation he has been indicated as the first author of the paper on AZO fiber based coatings.

III. The author prepared the samples for the fluorescence measurements and took an active part in the optical measurements of fluorescence and light scattering from the samples. The author actively participated in the analysis and discussions of the obtained results and their description in the paper. It is worth noting that the author proposed a spectacular way of representing the angular dependences of fluorescence in the form of two-dimensional contour plots, which were put into the article as the most illustrative ones.

IV. The author participated in the scientific discussions on the stages of interpretation of the results and preparation of the paper about usage of gold nanoparticles as nanostructures providing surface enhanced Raman scattering. However, this paper is not directly related to the main results of the thesis.

## INTRODUCTION

This investigation is focused on processing and characterization of transparent electrode materials based on Al-doped zinc oxide (AZO). Transparent electrodes are thin transparent conductive films (TCFs), which are optically transparent and electrically conductive. They have usually been fabricated from transparent semiconductive oxides (TCO). There are indium tin oxide (ITO), fluorine doped tin oxide (FTO), Al/Ga-doped zinc oxides. However, ITO is expensive and shortage of indium may occur in the near future because of the limited indium reserves in the world. AZO, FTO are indium-free alternative to ITO. ZnO-based TCOs are cheaper and due to their electrical and optical properties are capable to replace ITO for transparent electrode applications. Up to now, ZnO films are manufactured by different methods: pulsed laser deposition, electron-beam evaporation, molecular beam epitaxy, chemical vapor deposition, spray pyrolysis, sol-gel and others. Methods of film preparation imply the quality and price of the resultant films. As far as it is known, among the variety of methods there are not those, which are fully suitable for mass production. In connection with this, it is desirable to develop or improve a technique, which does not require complicated and expensive equipment. It is important for the potential application of indium-free TCFs in such optoelectronic devices as solar cells, light-emitting diodes, liquid crystal indicators and displays based on them. Performance of these devices is greatly dependent on the properties of the electrodes. For this reason, it is very important to improve manufacturing process and properties of TCFs.

Renovated interest to the preparation of optical materials by wet chemistry methods, such as sol-gel route, is due to the recent progress in related chemistry and technology. According to the data from the Global Industry Analysts Inc., the global market for the sol-gel products is forecast to reach 3.2 billion \$ by 2020 [1]. Such tendency is stipulated by comparatively simple, non-vacuum and low-cost sol-gel routes for preparation of optical materials, in which size, homogeneity and doping level can be properly controlled. So it turned our attention to possible application of sol-gel route for the preparation of transparent conductive oxides.

The core of the present work describes specially adapted sol-gel techniques, which allow to obtain AZO films with desirable optical and conductive properties. Special attention was paid for proper pre-treatment of substrates before the deposition of AZO films, control of temperature and composition of the precursors. Spin-coating and electrospinning methods were used for the deposition of the films.

Influence of aluminium content, annealing time/temperature, heating rate and annealing environment on the film resistivity and transmittance were investigated for the spin-coated films. Increase of films' thickness usually caused increase in their conductivity and decrease in their optical transmittance. In addition to the optical transmittance, moderate visible fluorescence from the

AZO films was detected at ultraviolet excitation and controlled through the special optical scheme. Namely, AZO film was deposited on the gilded glass attached to the semicylindrical prism. Obtained directional fluorescence was observable at resonant angles. It was associated with coupling of fluorescent light with hybrid waveguide-plasmonic and waveguide modes propagating along the AZO-gold interface. The judgements about these modes were done on the basis of calculated electric field distribution inside the AZO-gold layers.

There was proposed a modification of electrospinning method for preparation of fiber based films in different atmospheric conditions. Granulation and coalescence states of fibers at different annealing temperature, humidity and Al dopings were investigated. Concentration of Al dopant was varied by small steps in order to trace changes in electrical properties of the samples.

Prepared AZO films demonstrated acceptable conductivity and transparency in visible spectral range. The films prepared by spin-coating method were successfully examined as transparent conductive electrodes in the liquid crystal indicator. It testifies that the approach developed in current work is prospective for preparation of transparent AZO electrodes and their adaptation for the mass production.

# 1. BACKGROUND

## 1.1. Traditional and novel materials for transparent electrode applications

Transparent conductive electrodes are constitutive parts of such modern opto-electronic devices as light-emitting diodes, solar cells, light emitting and liquid crystal displays [2,3]. In these devices light is generated\absorbed in a solid structure and go out or go in through the electrodes. Because of this, one has to combine controversial properties such as low electrical resistivity, small thickness and high optical transmittance in a way to increase energy efficiency of the whole device. Additionally TCFs have to be cheap for mass production.

Transparent conductive electrodes are possible to divide into several groups, which differ by dominant or conductor material (metals [4,5],  $\text{In}_2\text{O}_3$ ,  $\text{SnO}_2$ ,  $\text{ZnO}$ ,  $\text{In}_2\text{O}_3\text{-SnO}_2\text{-ZnO}$ ,  $\text{In}_2\text{O}_3\text{-SnO}_2\text{-CdO}$  [6], polymers, nanotubes, graphene [7,8]). Each group has their advantages and disadvantages, which narrows down their potential applications from resistivity and transmittance point of view. When comparing TCFs' properties by absolute values, it necessary to note that film deposition or assembly can alter noticeably the key properties of films. Preparation methods will be described in section 1.5. Here we introduce typical materials.

TCFs based on metals are made from Al [9], Pt [5], Au [4] and some others. On the one hand, to achieve desirable transmittance, metal films have to be very thin (Figure 1.a). J. Siegel et al. reported in [4] that sputtered transparent gold films with transmittance above 60 % have a thickness less than 10 nm. On the other hand, very low film thickness leads to undesirable high sheet resistance [5] (Figure 1.b) or resistivity [10], where the last one is not constant and changes with film thickness as a consequence of its nano-dimension. Equation for conversion of sheet resistance to resistivity is presented in section 1.2. By varying these parameters with the deposition of additional layers of other materials  $\text{TiO}_2/\text{Ag}/\text{TiO}_2$  [11],  $\text{ZnO}/\text{Ag}/\text{ZnO}$  [12] it was possible to achieve more or less acceptable values of transmittance and resistivity at once.

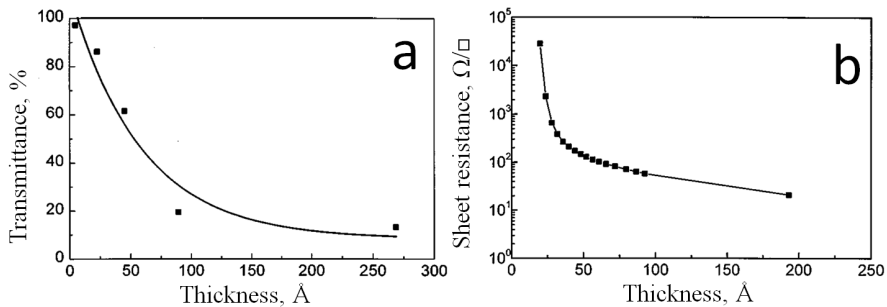


**Figure 1.** a) Transmittance and b) sheet resistance as a function of film thickness for Pt [5].

Next group of TCF's materials is represented by transparent conductive oxides (TCOs). They have a higher optical transmittance with acceptable resistivity compared to metals. TCOs usually are n-type wide band-gap semiconductors, where high conductivity can be obtained by means of doping. This group is represented in general by CdO,  $\text{In}_2\text{O}_3$ ,  $\text{SnO}_2$  and ZnO based materials.

CdO is a semiconductor with a face-centered cubic crystal structure and 2.19 eV band gap. CdO thin films have been made by using different methods such as magnetron sputtering [13], spray pyrolysis [14] and others. CdO doped by In, Sn, or F and complex compounds such as  $\text{CdSnO}_3$ ,  $\text{CdIn}_2\text{O}_4$  [3,6] have a good transmittance around 90 % and a low resistivity  $10^{-4} \Omega\cdot\text{cm}$  [15]. However, in reality application of Cd based films is very limited because of their high toxicity [16].

$\text{In}_2\text{O}_3$  is bixbyite-type cubic crystal structure semiconductor with band gap around 2.9 eV [3]. It was doped by many different dopants such as Sn, F, Zn, Ge, Ti, etc. Nevertheless, Sn-doped  $\text{In}_2\text{O}_3$  (ITO) became industry standard in TCFs. Despite the fact that ITO is defined as Sn doped  $\text{In}_2\text{O}_3$  [17,18], it also can be defined as a mixture of  $\text{In}_2\text{O}_3$  and  $\text{SnO}_2$ , where concentration of the last one is around 10 % [19,20]. It has resistivity around  $10^{-4} \Omega\cdot\text{cm}$  and transmittance above 80 % in the visible spectral range. Although ITO is widely used, it is expensive and shortage of indium may occur in the near future because of the limited world indium reserves [21]. For these reasons much attempts are focused on the development of ITO alternatives.

$\text{SnO}_2$  has body-centred tetragonal crystal structure and band-gap 3.62 eV [3]. Wide band gap makes  $\text{SnO}_2$  transparent even in the ultraviolet region. Tin oxide was doped with F [22], Sb, Nb, Ta, etc [3,6] to achieve desirable conductivity. From the range of dopants mentioned above F-doped  $\text{SnO}_2$  (FTO) has lower price and resistivity slightly higher than ITO. It makes F-doped  $\text{SnO}_2$  commercially attractive [23].

ZnO is a semiconductor, which has band-gap 3.37 eV at room temperature [24]. ZnO thin films have suitable electrical properties as well as a high transmittance. The latter is usually above 90 % in the visible spectral range. To achieve a low resistivity ZnO has to be doped with Al [25], Ga [26], F, In, etc [3]. Al-doped ZnO (AZO) and Ga-doped ZnO (GZO) are most remarkable for TCOs applications. ZnO-based TCOs are cheap and due to their electrical and optical properties are capable of replacing ITO as transparent electrode in applications [3]. AZO is cheaper compared to GZO and due to this it is more preferable. Even though AZO has good properties, it has been produced by expensive methods such as CVD [27] or sputtering [28]. Therefore current attempts are focused on the development of methods that would be inexpensive and more suitable for mass production.

Next group of TCFs is represented by ternary compounds such as  $\text{Zn}_2\text{SnO}_4$ ,  $\text{CdSnO}_3$  and alloy systems  $\text{In}_2\text{O}_3$ - $\text{SnO}_2$ -ZnO,  $\text{In}_2\text{O}_3$ - $\text{SnO}_2$ -CdO [6]. Due to the nature of the solid solutions it is possible to influence their conductivity and shift the band-gap in a specific range and consequently vary the transmittance

window. However, these multicomponent materials are difficult to deposit and further research in this direction is necessary.

We would like to note the existence of a few other materials that can potentially replace ITO. They include Ag nanowires, CNTs, graphene, conductive polymers (Figure 2). A good overview is given by McCoul et al. [29]. These materials can be deposited on stretchable/flexible substrates as well. They have a big potential but they are still under development.

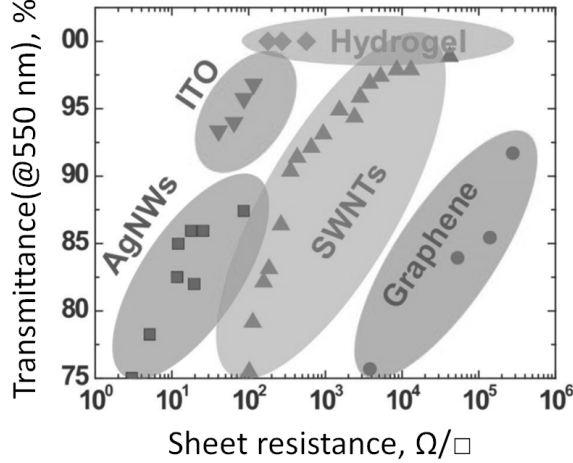


**Figure 2.** Sheet resistance of specific alternative materials and their transmittance at 550 nm wavelength [29].

From the above mentioned materials AZO is a promising indium-free alternative to ITO for mass production. It was prepared by sputtering [28] and demonstrated good results. To make deposition procedure cheaper sol-gel methods are preferable. In fact there are articles dated more than ten years ago, which represented good transmittance and resistivity of AZO films prepared by sol-gel method [30]. However, inability to reproduce their results in the lab or obtain films with similar or better properties by many groups years later [25,31,32] drive scientists for further research. In this work we are focused on preparation of thin AZO films from sol-gel solution by different routes and investigation of electrical and optical properties of the prepared samples.

## 1.2. Electrical properties of transparent conductive oxides

To achieve high conductivity semiconductor has to be doped by elements with higher or lower valence. Conductivity  $\sigma \left[ \frac{S}{cm} \right]$  in semiconductors can be expressed as [33]:

$$\sigma = en_0\mu_e + ep_0\mu_p, \quad (1)$$

where  $e$  is elementary charge [C],  $n_0$  and  $p_0$  are concentration of electrons and holes [ $\text{cm}^{-3}$ ],  $\mu_e$  and  $\mu_p$  are mobility [ $\frac{\text{cm}^2}{\text{Vs}}$ ] of electrons and holes, respectively. Charge carrier concentration is determined mainly by the doping level whereas mobility is determined by level of scattering charges on crystal structure and structural defects (including dopant atoms). In n-type semiconductors the concentration of electrons is much higher than the concentration of holes. Opposite situation is in p-type semiconductors. Usually only the main charge carrier concentration is taken into account in the equation mentioned above. In most cases the hole mobility is lower than the electron mobility [33]. Because of this using of n-type semiconductors is beneficial for reaching high conductivities in TCOs.

The type of charge carrier and its mobility are possible to determine by Hall effect. Because of this the mobility is also called Hall mobility  $\mu_h$ . The influence of dopant on the electron concentration (carrier density) and mobility in AZO films was measured by Wang et al. (Figure 3) [34]. Initially  $n$  and  $\mu_h$  increase with the concentration of dopant, and therefore conductivity increases also. When the level of dopant reaches certain critical level, the mobility (and also conductivity) starts to decrease as a consequence of increased scattering.

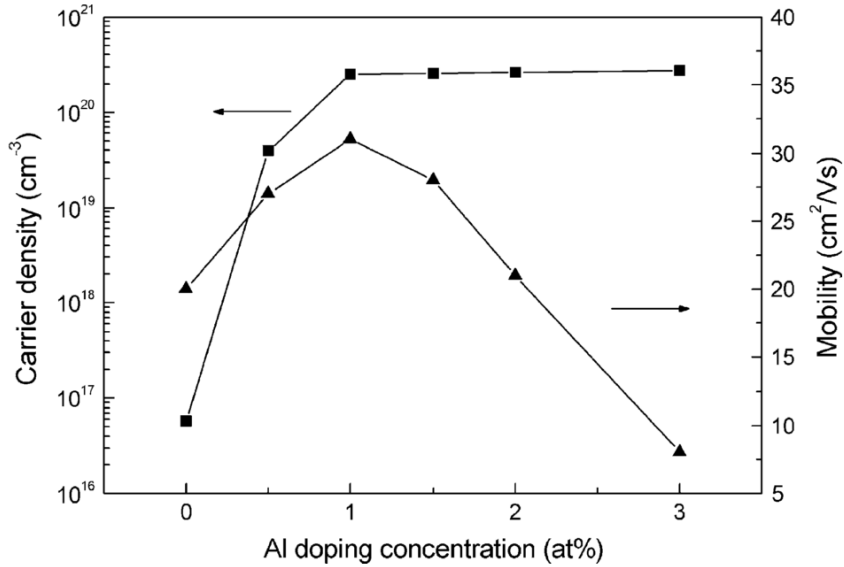


**Figure 3.** Carrier concentration ( $n$ ) and the Hall mobility ( $\mu_h$ ) of AZO films annealed at 500 °C as functions of Al doping concentration [34].

According to the dependence of mobility on temperature it is possible to determine dominant scattering mechanism in a particular non-heavily doped TCO.  $\ln(\mu) \sim -T^{-1}$  is typical for scattering on grain boundaries [35].  $\mu \sim T^{-1}$

is typical for scattering on phonons [36].  $\mu \sim T^{3/2}$  is typical for scattering on ionized impurities [37]. In heavily doped TCO the scattering on ionized impurities is dominant and independent of temperature at low temperatures [36,37].

As the scattering of electrons on any kind of defects has significant impact on electrical properties of semiconductors, it is extremely important to use high quality precursors and carefully choose the preparation method in order to get desirable resistivity.

In field of TCFs sheet resistance  $R_{\square}$  [ $\Omega/\square$ ] and resistivity  $\rho$  [ $\Omega \cdot \text{cm}$ ] are widely used instead of conductivity, where  $\rho = 1/\sigma$ . Sheet resistance  $R_{\square}$  and resistance  $R$  [ $\Omega$ ] of bulk material wire are related by the formulas:

$$R = \rho \frac{L}{S} \Rightarrow \rho = R \frac{S}{L} = R \frac{ta}{L}; \lim_{a \rightarrow L} \rho = R_{\square} t, \quad (2)$$

where  $L$  is a length of the wire,  $S$  is a cross-sectional area of the wire, which has thickness  $t$  and width equal to  $a$  (Figure 4). Here  $R_{\square}$  has the same meaning as  $R$  and  $\square$  indicate that resistance was measured for sample with equal width and length or in other words for square with finite thickness. If we know sheet resistance of one square piece  $R_{\square} = R_i$ , it is easy to calculate the resistance of the whole sample consisting of  $n$  of such square pieces:  $R = \sum_1^n R_i = R_{\square} [\Omega/\square] \cdot n[\square]$ . This is the main difference between  $R_{\square}$  and  $R$ , and to distinguish them the units of  $\Omega/\square$  were introduced [38].

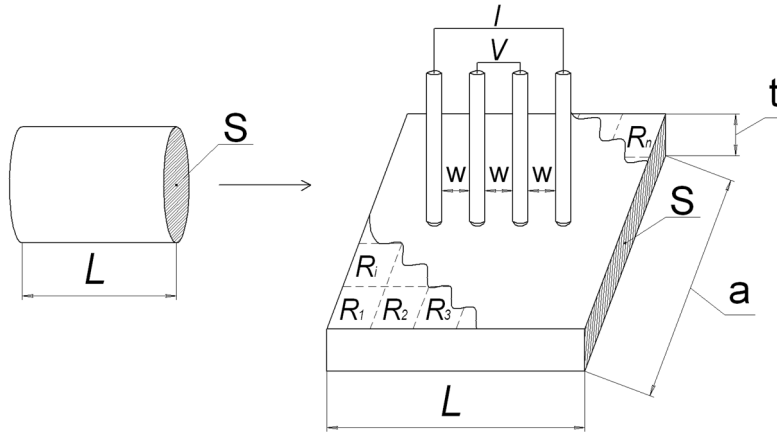


**Figure 4.** A piece of bulk wire with resistance  $R$  (left) and thin film (“mashed wire”) with sheet resistance  $R_{\square} = R_i$  of one square piece (right). Probes on the top of the film are for the four-point probe measurements.

In practice, for measurement of sheet resistance four-point probe method is widely used. It allows elimination of sometimes significant parasitic resistance



from wires connected between source-meter and probes. The theory of the four-point probe method is developed by Smits [39]:

$$\rho = \frac{1}{\sigma} = R_{\square}t = \frac{\pi}{\ln(2)}F \cdot \frac{V}{I} \cdot t \approx 4.532 \frac{V}{I} \cdot t, \quad (3)$$

where  $t$  is film thickness [cm],  $V$  is voltage [V],  $I$  is current [A],  $F$  is a correction factor [39]. For this measurement the current  $I$  is fixed and the voltage  $V$  is measured. The distance between the probes is fixed and equal to  $w$  (Figure 4). The right part of the formula is valid if  $L \gg w \gg t$ , otherwise the correction factor  $F$  has to be used. Additional information about the four-point probe method and probe configurations can be found in Ref. [38].

It is important to note that non-contact sheet resistance measurement techniques also exist. They are based on eddy current testing [40] and commercially available [41]. It can be significant for structures such as graphene. Discussion of these methods is beyond the scope of this work.

### 1.3. Optical properties of transparent conductive oxides

This section describes only the basic optical properties and their connection with the electrical ones with the aim to highlight the development of TCOs. More detailed overview can be found in Ref. [3,6].

Typical transmittance spectrum of well-developed TCO is represented in the Figure 5. Transmittance is maximal in the visible spectral range, whereas it is very low or zero in the near ultraviolet (UV) and near-infrared (NIR) regions. The transmittance in the near-UV region is limited by the effective band-gap  $E_g$ , where photons with bigger energy are absorbed [42] and transmittance drops abruptly. In the NIR region the transmittance is generally limited by the reflection at the plasma frequency. The transmission window is in the region between these two diapasons, where light is going mostly through the material. The doping level noticeably changes charge density, which is connected with plasma frequency and effective band gap (Burstein-Moss effect) [43]. Because of this the transmission window becomes narrower in the NIR region and slightly shifted to the near-UV region in response to the increasing level of doping. Shift in the NIR region is predominant. Interference fringes in the transmission window can be associated with reflections from surfaces and interfaces, film thickness and incident wavelength, which can be used to achieve higher transmittance in TCOs [3].

In addition to chemical composition and material purity, it is possible to control optical properties of TCOs by variation of film thickness, thickness uniformity, and surface roughness [42].

By considering electrical and optical properties together it becomes clear that a lower resistivity narrows the transmission window. Following this further, it is important to take into account the particular application of TCFs to maxi-

mize the efficiency of the whole device. For example, for LED structures it is important to have maximal transmittance basically in visible spectral region, whereas for solar cells having wider transmission window is more significant [3]. Also it is possible to increase the film thickness to decrease the sheet resistance, however it decreases transmittance and, in this sense, acceptable compromise has to be found.

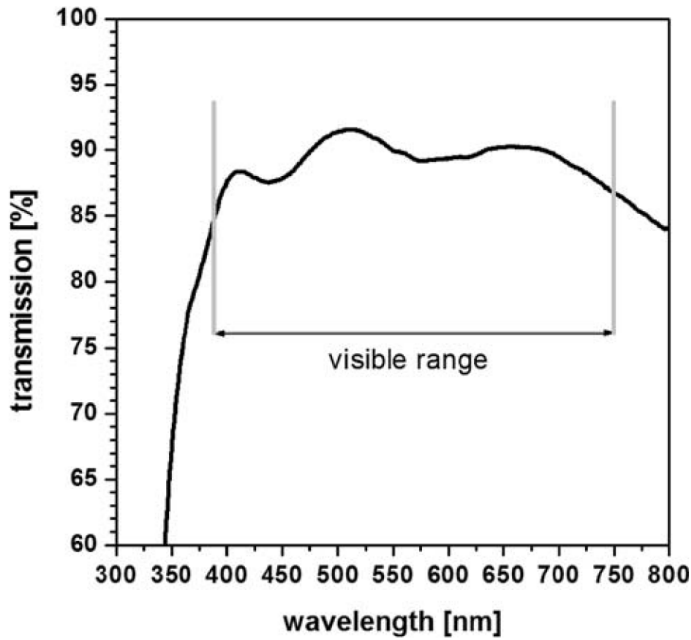


**Figure 5.** Transmittance spectrum of an ITO film with a thickness of 500 nm [44].

## 1.4. Highlights of the particular applications of AZO structures tested in this work

### 1.4.1. Possibilities to control the fluorescence of AZO structures

As it was mentioned above, the optical usage of TCOs in general and AZO in particular supposes their ability to transmit light, which is not reflected by the film surfaces or absorbed inside the film. However, if the film exhibits fluorescence, it not only transmits light, but also can generate it. AZO films have a moderate own fluorescence with characteristic spectral bands in the near ultra-violet and visible spectral ranges. As a direct gap semiconductor, zinc oxide has a characteristic edge luminescence in a spectral range near 400 nm and a defect related luminescence with maximum near 520 nm [45]. Consequently, the edge

luminescence could be interesting for the lasing applications in the violet or ultraviolet spectral range [46]. The control of defect-related luminescence can be interesting for the single photon light sources and optical communication lines [47]. An overview of the specific possibilities to control this fluorescence is represented below. The original experimental results concerning the control of AZO fluorescence are represented in section 4.3.1.

In multilayered coatings the control of light can be achieved via interference effects or via coupling of light with specific plasmon-polariton waves at the metal-non-metal interface. In both cases the rates of absorption or fluorescence processes can be increased, either by the electric field of surface plasmon-polariton wave localized at the metal-non-metal interface (Figure 6.a) or by electric field of the light guided/leaked in/from the layer (Figure 6.b).

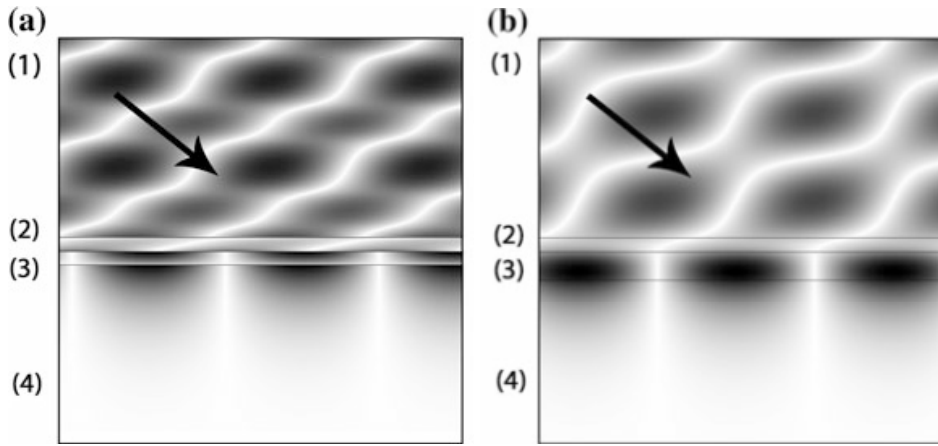


**Figure 6.** Calculated diagram of electric field distribution in a layered structure: (1) glass, (2) gold, (3) titania, (4) air. The thicknesses of titania layer are different: (a) 47 nm, (b) 100 nm. Arrows indicate the direction of incident light. Picture is reproduced from Ref. [48].

The difference is only in the degree of field localization. Electric field is usually stronger localized at the metal-non-metal interfaces (Figure 6.a), because the surface plasmon-polaritons propagate mainly along these interfaces. Their electric field is concentrated near the interface and penetrates inside the material only at the distances, which are not larger than several tens of nanometers [49]. It is because of an exponential decay of surface wave away from the interface. However, surface plasmon-polariton waves suffer from the damping and loss of energy in the metal. Therefore the multilayered non-metal coatings with less losses are used if compromise in field localization is acceptable [50]. Theoretical estimations testify that using layered coatings and plasmonic structures can result in up to 10 % increase in the efficiency of photovoltaic devices [51]. Experimental results about the solar cells based on

AZO coatings doped by noble metals confirm the prospects of this estimation [52].

The wave vector of a freely propagating light is less than the wave vector of surface plasmon-polariton. Therefore excitation of surface waves and their coupling with fluorescence is possible only when the wave vector of light becomes equal to the wave vector of surface wave. Experimental discovery of these conditions was done by E. Kretschmann [53]. The physical implementation requires passing the light through a prism with sufficiently high refractive index  $n$ , which results in the  $n$  times increase in the wave vector of light (Figure 7). The incident angle of light in the prism was adjusted so as to achieve the total internal reflection providing the necessary electric field distribution of the so-called evanescent wave, which exponentially decays away from the interface [54].

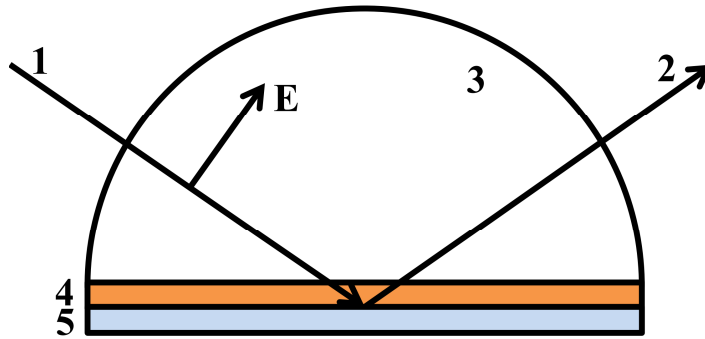


**Figure 7.** Kretschmann scheme: (1) incident light beam; (2) detected light beam; (3) semicylinder prism; (4) gold layer; (5) non-metal film. An arrow  $E$  together with the light beam (1) forms the plane of electric vector oscillations in case of the p-polarized light. It was shown that only p-polarized light can generate surface plasmon-polariton wave, because only electric field of the p-polarized light has a component normal to the interface (4)–(5) and able to induce the non-compensated electrical polarization of the surface.

The scheme proposed by E. Kretschmann appeared so fortunate that it was used in several applications. Particularly, it allowed changing the spectral shape, intensity and angular distribution of fluorescence from organic fluorophores, which can be used to increase the sensitivity in fluorescence microscopy [55, 56]. The scheme appeared useful for the detailed study of coupling of fluorescence with plasmons and obtaining coherent plasmons [57,58], which opens the way for the plasmon lasers working below the optical diffraction limit.

The original results of this work are devoted to the control of AZO fluorescence realized by means of reverse Kretschmann scheme represented in section 4.3.1.

### 1.4.2. Use of AZO films in the liquid crystal indicators

The AZO films described in section 4.1 were tested as conductive layers for the liquid crystal indicator. Since using of AZO electrodes implies understanding of the indicator working principle, the construction of such indicator is described below.

Liquid crystals can be also named as anisotropic liquids. Optically this anisotropy can be used in the liquid crystal indicators and displays for obtaining the pixels with bright or dark appearance forming an image. Further addition of colour filters and back lighting supplies formation of colour images [59].

The aligned layer of rod-like liquid crystal molecules has birefringent properties similarly to a uniaxial crystal. It means that the incident polarized light beam coming through such layer is divided into two beams with perpendicular polarizations: so-called ordinary and extraordinary beams. An analyzer brings the electric vectors of these beams into one plane allowing them to interfere. Constructive or destructive interference will result in brighter or darker final pixel (Figure 8).

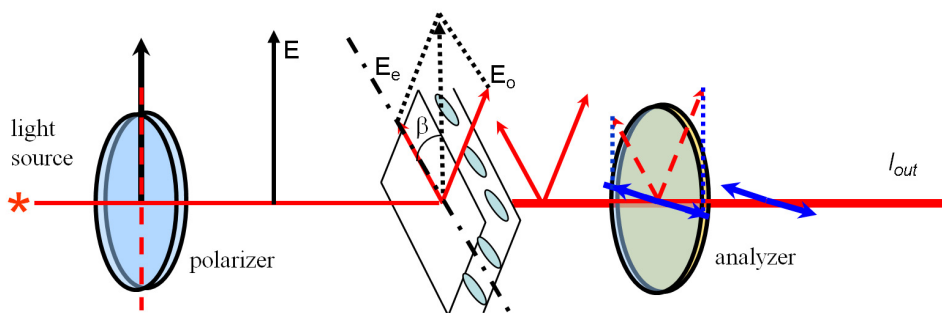


**Figure 8.** Path of a light beam through a uniaxially oriented liquid crystal layer placed between crossed polarizers.  $E_o$  and  $E_e$  are electric field strength vectors for ordinary and extraordinary light beams. Blue arrows show the interfering electric vectors, which are brought together in the horizontal plane by the analyzer.

The changes in brightness are achievable by applying different voltages to the liquid crystal layer. Due to different permittivity of liquid crystal molecules along and across their axes, the molecules can be oriented in parallel (positive liquid crystal) or perpendicular (negative liquid crystal) to the applied electric field and by such a way change the light interference and brightness of liquid crystal layer set between the crossed polarizers.

Since the times, when the first liquid crystal indicators appeared, a lot of efforts have been applied to make them cheaper, working at smaller voltages and in broader temperature intervals, make them faster, improve the contrast, colour and flexibility [60]. Current products in the market combine elegant technological solutions with advanced knowledge in the chemistry of different

liquid crystal materials, surface physics and surface chemistry allowing to achieve better initial orientation and pretilt angle of liquid crystal molecules, which are important for the quick switching and absence of image sticking effects. The works in this field are in continuous progress and liquid crystal displays are in continuous competition with light emitting diode displays and electrophoretic electronic paper [61,62].

Current liquid crystal indicators frequently use twisted orientation of the liquid crystal layer. Switching in such twisted structure is quicker, because of an additional torque elasticity imposed to the liquid crystal layer in such configuration. Structurally, the liquid crystal molecules adjacent to the top and bottom substrates have perpendicular orientation in the initial state (Figure 9). The molecules are oriented along the grooves specially made in aligning polymer layers by their directional rubbing with fleecy cloth. The electric vector of the transmitted light is twisted by such a way to follow the direction of liquid crystal alignment in the off-state at appropriate thickness of liquid crystal layer. Therefore the cell set between the crossed polarizers transmits light in the off-state (Figure 9.a). Molecules reoriented along the applied conductive surface electric field do not support rotation of electric field strength vector inside the liquid crystal layer. Therefore the on-state of cell looks dark in crossed polarizers (Figure 9.b).

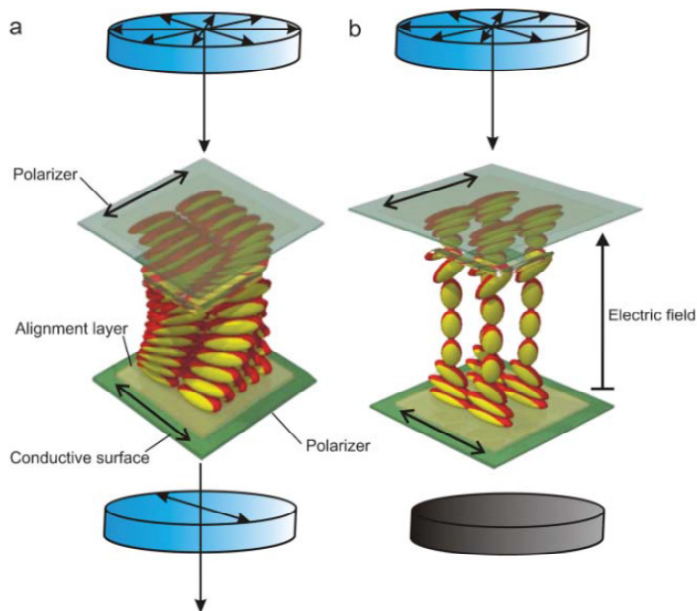


**Figure 9.** Scheme of twisted-nematic liquid crystal cell: (a) off-state; (b) on-state. The picture is reproduced from [63]. Here the conductive surface can be replaced by AZO.

Substrates for liquid crystal cells should be sufficiently transparent and simultaneously conductive providing on the one hand good transmittance and on the other hand switching at comparatively low voltages. Alternatives to the indium containing conductive layers are necessary to substitute indium for less expensive materials such as AZO [64] or graphene [65].

AZO films deposited by the magnetron sputtering showed a promising performance as conductive layers for the liquid crystal indicators [64]. However, to the best of our knowledge there is no data about the performance of liquid crystal indicators based on AZO films prepared by means of sol-gel method. The structure and behaviour of twisted-nematic liquid crystal cell based on sol-gel AZO films are described further in section 4.3.2.

## 1.5. Preparation methods of transparent conductive oxides

Since sol-gel method is applied here for preparation of TCO coatings, it is reasonable to overview shortly its place among other approaches. Transparent conductive oxides have been prepared by many methods and some of them are still under development. A short overview of the results achieved by different methods is represented in Table 1. It is easy to see that the properties of the obtained samples vary significantly from method to method. One of the main reasons for existence of such variety of methods is their different cost. On the other side, it is desire to obtain films with better properties in particular cases, when the cost is of secondary importance. For example, the best results were achieved by molecular beam epitaxy. However, it is not suitable for mass production, because of the high cost (including the energy expenses) [3]. For these reasons development of cost effective methods for preparation of TCO films is actual.

**Table 1.** Properties of TCOs prepared by different methods.

Material	Preparation method	Resistivity, $10^{-4}\Omega\cdot\text{cm}$	Transmittance at 550 nm, %
ITO	“Commercial” [23]	~1	>85
	Sputtering [66]	~1.2	>80
	Sol-gel [20]	23	>90
FTO	Spray pyrolysis [22]	~4	>85
GZO	MBE[26]	~1	>90
	CVD[27]	27	>90
AZO	CVD [27]	~1	>90
	Sputtering [28]	~6	>90
	Spray pyrolysis [67]	~10	>90
	Sol-gel[32,68]	14-200	>90

In this work we are focused on the preparation of thin AZO films from sol-gel solution as one of the most promising method for mass production. Despite of the variety of published articles describing preparations of films by sol-gel method, it is very common fact that it is frequently impossible to reproduce the published results in the lab. It can be caused by the reason that the description of some experimental steps are just skipped in the publications by assuming that these steps are self-evident or not important. It can be also that after successful preparation some important parameters were not documented very carefully. For this reason reproducibility is the second important factor in film preparation by this method.

Compared to other methods, sol-gel process has several benefits. It is simple, non-vacuum and low cost technique that does not require utilization of complicated and expensive equipment. This process gives opportunity to produce both small and large area coatings of desirable shape at relatively low temperatures. Moreover, there is an easy way to control solution concentration, doping level, and homogeneity. Usually, the resulting films are uniform and have a high purity. However, it is necessary to find and use the optimized processing parameters that are required for minimization or elimination of effects related to film shrinkage and film cracking.

Sol-gel basics are well described in a work of Brinker [69]. A good review of the sol-gel preparation of ZnO films is represented by Znaidi [70], however he did not provide any connection to the properties relevant for TCO applications, such as transmittance or resistivity. The typical scheme of preparation of ZnO films is represented in Figure 10. According to Znaidi it is possible to indicate three important technological steps: preparation of the precursor solution; deposition of the prepared sol on the substrate by the chosen technique; and heat treatment of the xerogel film. The xerogel is the gel dried at ambient pressure. The details of these steps and the processing parameters for AZO films formation will be discussed in sections 3 and 4.1.



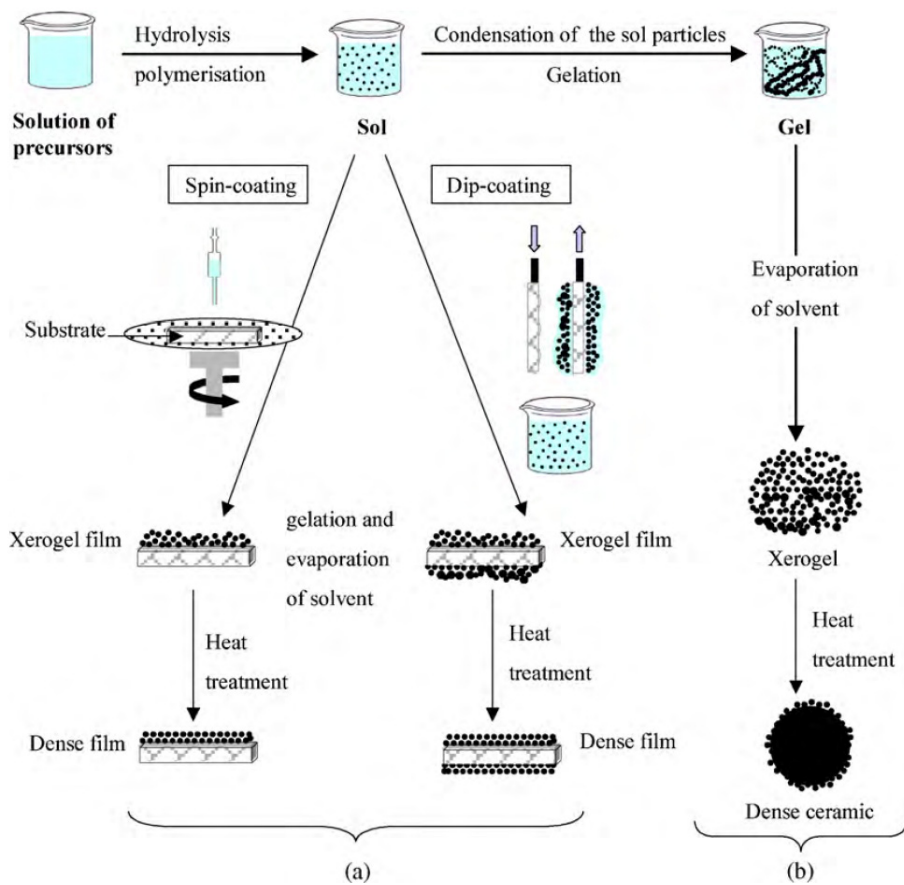


**Figure 10.** An overview of the sol-gel method showing two synthesis examples; (a) films from colloidal sol; (b) powder from colloidal sol transformed into a gel [70].

## 2. GOALS OF THE RESEARCH

Limited amount of indium, which is currently widely used in the transparent conductive electrodes, stipulated the search of alternative materials. It is hard to solve the problem even with the help of such actual material as graphene, because sheet resistance of the neat graphene is not sufficiently low to substitute indium tin oxide. Since some prospects are connected with the zinc oxide doped by aluminium (AZO) coatings, the goal of this research is elaboration of relatively inexpensive sol-gel based methods for preparation of such coatings and investigation of their electrical and optical properties. The goal included also an applied aspect in a sense that the prepared AZO films were aimed to be tested as a part of electro-optical liquid crystal indicators and AZO-gold structures prospective for the fluorescent reflective type displays and optical sensors.

In spite of certain amount of publications related to the AZO, there is no systematic data about the dependence of their properties on the preparation conditions, especially in case of sol-gel method. Partly it is caused by the fact that different authors controlled different preparation parameters in different ranges or certain experimental conditions are not described in all details. So the author was faced with the necessity to reconsider critically the existing sol-gel approaches for the preparation of AZO films and elaborate own recipes. During the implementation of this goal it was revealed that even changes in the ambient humidity or heating rate of the samples led to alteration of their electrical and optical properties. Thus, realization of the pointed goal required a thorough investigation of all steps of the sol-gel preparation procedure, practical preparation and thermal treatment of samples in different atmospheres, analysis of their physicochemical properties. There were prepared both spin-coated continuous AZO films and fiber-based samples by means of electrospinning. Finally, specific behaviour of fluorescent and reflected light in structures, which include AZO films, was investigated and the performance of the AZO films as conductive layers in the liquid crystal indicators was tested.

### 3. EXPERIMENTAL FACILITIES

This section describes materials, methods and experimental equipment used for the preparation and characterization AZO films as well as AZO based liquid crystal cells. Major preparation steps of AZO films by means of sol-gel deposition via spin-coating and electrospinning techniques are shown in Figure 11.

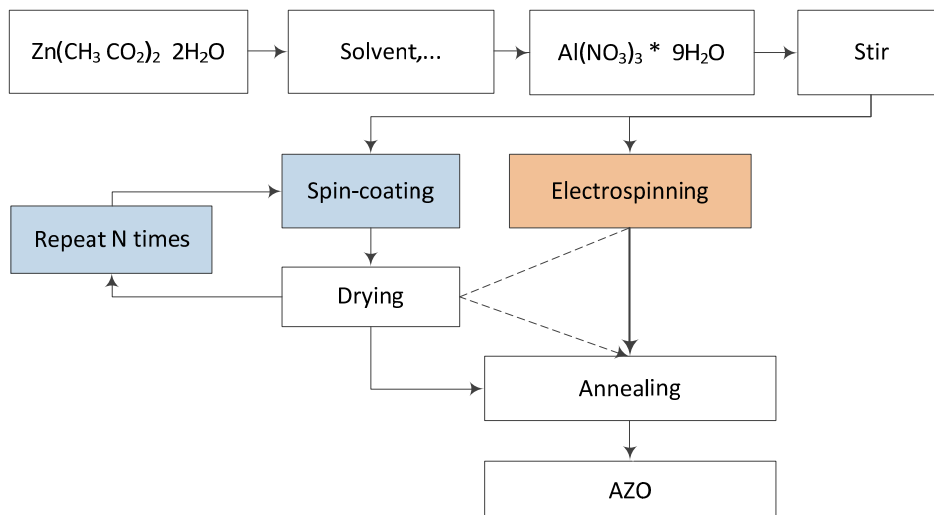


**Figure 11.** Major preparation steps of AZO films by spin-coating and electrospinning techniques. White boxes indicate steps common to both methods.

#### 3.1. Synthesis of AZO films by spin-coating method

Two different AZO solutions were prepared (subsequently called as routes #1 and #2). For the synthesis zinc acetate dihydrate  $[\text{Zn}(\text{CH}_3\text{CO}_2)_2 \cdot 2\text{H}_2\text{O}]$  (Sigma-Aldrich, assay  $\geq 99\%$ ), 2-methoxyethanol  $[\text{C}_3\text{H}_8\text{O}_2]$  (Sigma-Aldrich, assay  $\geq 99.5\%$ ), ethanolamine  $[\text{MEA}, \text{C}_2\text{H}_7\text{NO}]$  (Sigma-Aldrich, assay  $\geq 99\%$ ), aluminium nitrate nonahydrate  $[\text{Al}(\text{NO}_3)_3 \cdot 9\text{H}_2\text{O}]$  (Sigma-Aldrich, assay  $\geq 98\%$ ), ethanol  $(\text{C}_2\text{H}_5\text{OH}, \text{assay} \geq 99\%)$  were used. For convenience of the reader major technological steps are represented in Figure 11 and the details are described in section 4.1. The precise amounts of used precursors are shown in Table 4.

The samples were spin-coated by SCS-G3P-8 Spin Coater. After that the samples were put in a preheated hot chamber for drying. It led to a temperature fluctuation around  $20^\circ\text{C}$  in the moment when chamber was opened. To achieve a lower temperature fluctuation the oven chamber was replaced by hot plate. The hot plate was represented by heavy thick aluminium disk on the top of magnet stirrer (Figure 12.a). Heating power was set via magnet stirrer knob. A

thick heavy disk was used for temperature stabilization. The real temperature was measured by independent thermometers operating in a wide range. In this case the temperature fluctuation was around 1 °C when a cold sample was put on top of the disk.

During the annealing traces of previously annealed substances can evaporate from the walls of the ceramic chamber. It led to differences in properties of the resultant films. For this reason the hot chamber was replaced by electrically heated quartz tube (Figure 12.b). Additionally, it allowed increasing the heating and cooling rates which in the case of the ceramic chamber was limited. Temperature was controlled via Eurotherm controller. Following this further it was developed special aluminium-rubber details. They connect ends of the quartz tube with Supelco rotameter from one side and gas washing bottle from another to allow annealing samples in different atmospheres. Supelco Rotameter 23320-U was used for controlling the Ar or Ar:H<sub>2</sub> gas flow speed from the gas cylinder.

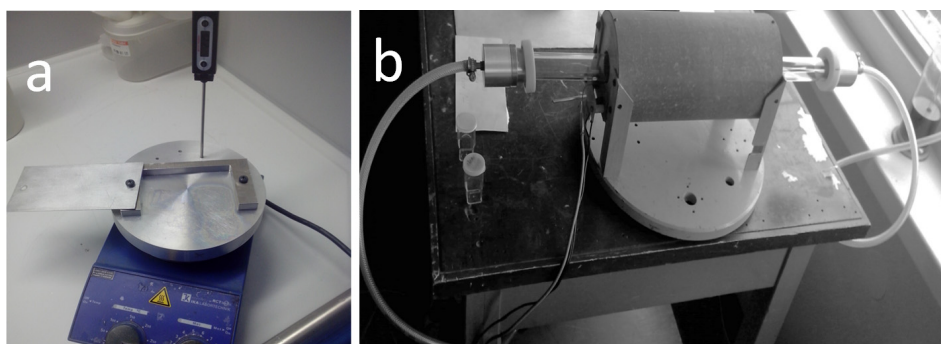


**Figure 12.** a) hot-plate set-up for drying the as-prepared samples; b) electrically heated quartz tube set-up for annealing the samples in different atmospheres.

### 3.2. Synthesis of AZO films by electrospinning method

The following components were used for the preparation of sol-gel precursor: deionized water, 2-methoxyethanol [C<sub>3</sub>H<sub>8</sub>O<sub>2</sub>] (Sigma-Aldrich, assay ≥99.5 %), zinc acetate dihydrate [Zn(CH<sub>3</sub>CO<sub>2</sub>)<sub>2</sub>·2H<sub>2</sub>O] (Sigma-Aldrich, assay ≥99 %), aluminium nitrate nonahydrate [Al(NO<sub>3</sub>)<sub>3</sub>·9H<sub>2</sub>O] (Sigma-Aldrich, assay ≥98 %), polyvinylpyrrolidone [(C<sub>6</sub>H<sub>9</sub>NO)<sub>x</sub>] (Sigma-Aldrich, Mw 360,000). For convenience of the reader the major technological steps are shown in Figure 11 and the details are described in section 4.2. The precise amounts of used precursors are shown in Table 5.

The scheme of home-made electrospinning set-up is shown in Figure 13. The potential difference via the power supply (h) (~ 25 kV) was applied to the two metal disks forming a uniform electric field in the region of fiber formation.

Sample was attached to the left metal disk (collector) (a) covered with aluminium foil. The piston of the syringe (e) with polymer solution was pushed by the pump (i) in order to form a droplet at the end of the needle. The electric field deformed a droplet into a Taylor cone [71]. When the surface tension forces become lower than electric forces the polymer jet arises from the Taylor cone. Such kind of jet reaches to the collector and sticks to it in the form of a fiber. So after some time of deposition a network from overlapped fibers forms a layer on the collector.

In order obtain reproducible fibers it was very important to pay attention to all of the following parameters: solution properties (polymer molecular weight [72], viscosity [73], surface tension [72,74] and conductivity [75,76]), process parameters (voltage [72,76], feeding rate [75,77], collector type [78–80], distance [76,81]) and ambient parameters (humidity and temperature [82,83]).

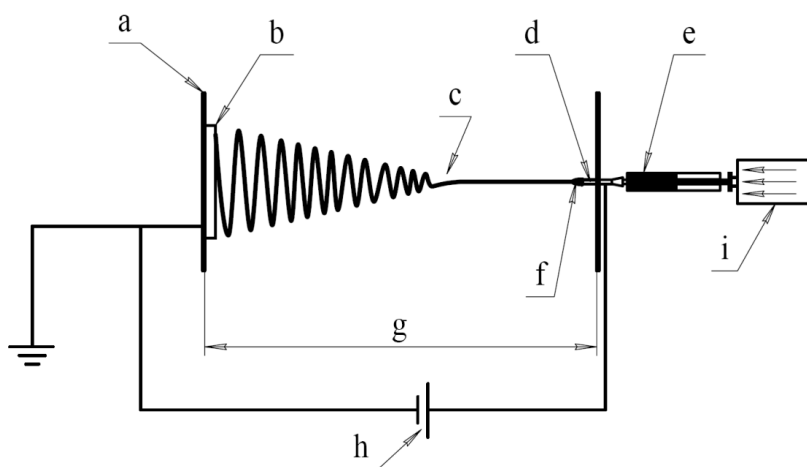


**Figure 13.** Home-made electrospinning set-up: a) metal disk (collector) b) sample c) fiber jet d) needle e) syringe with solution f) Taylor cone g) distance h) high-voltage power supply (LNC 30000-2pos; Heinzinger) i) syringe pump (Multi-Phaser NE-500; New Era).

### 3.3. Preparation of AZO-gold samples for the resonant control of fluorescence

AZO films were deposited by spin-coating method (as described above) on the glass slides and glass slides covered by 50 nm thick gold layer (Phasis company).

The AZO samples deposited on the gilded glass were attached to a semicylindrical glass prism by means of immersion oil (Figure 33). Such so-called Kretschmann scheme [84] allows observation through the prism of the reflected and fluorescent light from the AZO-gold interface. Laser light with wavelength 532 nm was incident through the prism and its reflection was collected also on

the side of the prism in the so-called Kretschmann geometry, whereas the excitation of the fluorescence was done on the side of the AZO film in the so-called reverse Kretschmann geometry [85]. It allowed to compare angular dependencies of the intensities of the reflected and fluorescent light. The exciting lasers were selected specially to allow such comparison. The ultraviolet 355 nm laser line was used because it effectively excited green fluorescence in the AZO films. The maximum of this fluorescence fell on the spectral range 530–540 nm. The laser line 532 nm was selected for the reflection measurements, because it is within the mentioned spectral range and gives a possibility to judge about reflection and fluorescence data in the same spectral diapason. The intensity of light was detected through the prism at different angles  $\phi$ .

### **3.4. Preparation of AZO films for liquid crystal cells**

Liquid crystal indicators based on the AZO films were prepared in following sequence. Glass substrates with AZO films (13 layers deposited by spin-coating method) were covered by a layer of rubbed planar polyimide JALS (Nissan). Twist cell (Figure 9) with thickness 10  $\mu\text{m}$  was assembled and filled by capillary flow with positive planar liquid crystal ZLI 4792 (Merck) having the elastic constants  $K_{11} = 13.2 \cdot 10^{-12}$  N,  $K_{22} = 6.5 \cdot 10^{-12}$  N,  $K_{33} = 18.3 \cdot 10^{-12}$  N and dielectric anisotropy  $\Delta\epsilon = 5.2$  (data are taken from Merck datasheet). Referent twist nematic cell with the similar parameters, but based on the indium tin oxide electrodes was used for comparison.

### **3.5. Substrate preparation**

Before deposition of films, the glass, Si and aluminium foil substrates were ultrasonically cleaned in acetone and methanol for 10 minutes, dried in a flowing nitrogen gas and finally cleaned in plasma cleaner for 10 min.

Clean substrates were stored in distilled water. Before deposition they were dried on hot plate at 250 °C.

### **3.6. Equipment used for the characterization of prepared samples**

The sheet resistivity was measured by using a four-probe method (Keithley 2400 sourcemeter). Film transparency was measured by using spectrophotometer Jasco V-570. Film thicknesses were measured by using electron microscopy (Helios NanoLab, FEI). Before annealing the nanofibers were inspected with optical microscope (Eclipse E200; Nikon). Shape of nanofibers and surface morphology of AZO films were measured by using electron microscopy (HR-SEM; Helios Nanolab, FEI). Element analysis was performed by using energy dispersive X-ray spectroscopy (EDS; Oxford Instruments). In order to deter-

mine resultant crystal structure of continuous AZO film, XRD and GIXRD analysis were performed on SmartLab (Rigaku) diffractometer. The incident angle for GIXRD analysis was  $0.4^\circ$ .

The fluorescence of the AZO and AZO-gold films were excited by using the third harmonic of a pulsed Nd:YAG laser (355 nm, 10 kHz). Angular dependences of light reflection for the AZO-gold films were measured by using the second harmonic (532 nm) of a continuous-wave Nd:YAG laser. Intensity of light was detected through the prism at different angles  $\phi$  by means of a fiber-coupled Andor SR303i spectrometer equipped with an Andor Newton CCD camera.

Transmittance of liquid crystal cells placed between crossed polarizers was investigated under application of an external voltage from 0 to 10 V at frequency 2 kHz from a home-made generator. A 635 nm diode laser with output power 5 mW was used as a light source in the transmittance measurements.

## 4. RESULTS AND DISCUSSION

To the best of our knowledge, there are currently no standards related to the preparation of AZO films from sol-gel solution with desirable structure, transmittance and resistivity. As it was pointed in section 1.1, there are several approaches, where variation preparation parameters such as initial precursors, concentration of dopant or annealing conditions have been studied. As a result, further variation in crystallinity, electrical or optical properties have been analysed. Different scientific groups use different ranges and steps in the variation of these parameters. Furthermore, it is hard to compare the properties of materials obtained by different authors and reproduce their results in the laboratory.

Our approach is more systematic and in this sense parameters such as concentration of Al dopant, humidity during the deposition of samples, temperature, atmosphere and heating rate at annealing, reproducibility were under control. The properties of continuous AZO films and nanofiber based films are described. Optical effects accompanying with the use of the AZO films in certain optical structures were investigated also.

### 4.1. Continuous AZO coatings: preparation features, electrical properties and light transmittance

Desirable properties for AZO films can be achieved on the one hand by selection of proper precursors and on the other hand by tuning, sometimes in a very delicate manner, the preparation conditions. In this sense the properties of samples are inseparable from the preparation routes, which were selected in an original way to improve the properties of final AZO samples. Here the main features of our approaches are described.

The two routes presented in this section were developed for preparation of AZO samples by sol-gel method. The route, where zinc acetate dihydrate was used for the sol precursor without any stabilization, will be referred to as route #1. It resulted in AZO films having large particles on the surface. Possibilities for preparation of films with small particles were also investigated. For this purpose ethanolamine was added to the precursors from route #1. This addition together with variation of preparation parameters was grouped and will be called route #2. As a result, structures with small particle on top were obtained. The details of the preparation procedures and the stipulated properties of the samples are discussed below.

In route #1 zinc acetate dihydrate and aluminium nitrate nonahydrate were dissolved in ethanol. Solution in capped bottles was refluxed by magnetic stirrer at temperature above 73 °C. Mixing time, speed and temperature have an effect on the homogeneous distribution of gelation centers in the solution. The optimal mixing speed was found to be near 1500 rpm. It resulted in a more homogeneous solution with only a small amount of microsized particles (Figure 14.a). In contrast, a lower mixing speed resulted in more grainy material (Figure 14.b).



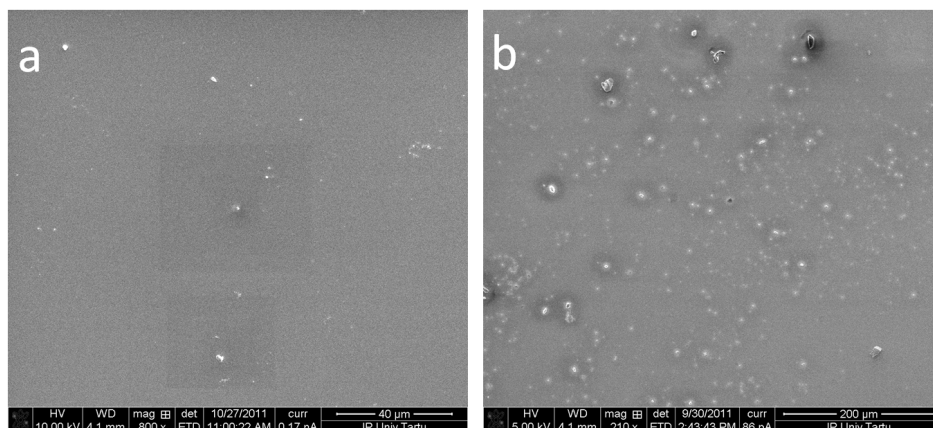


**Figure 14.** SEM images of dried films demonstrating the influence of solution mixing speed on the surface structure: (a) 1500 rpm and (b) 300 rpm. Route #1.

Thoroughly mixed solution was ready for deposition on clean substrates. The surface of the substrates was determinative for quality of the resulting coatings. Any dust or defects on the surface can lead to film deformation and cracking. Several experiments demonstrated that the optimal cleaning sequence should include ultrasonic treatment of substrates in acetone and methanol for 10 minutes, drying in a flowing nitrogen gas and final cleaning in atmospheric plasma for 10 min. RC1 and piranha solution cleaning methods were also tested but they did not give any benefit in resultant film quality.

The prepared solution was spin-coated on the soda-lime glass and Si substrates. The spin-coating step was repeated several times for obtaining thicker films. In this case intermediate drying of the just deposited layer was done at 260 °C in order to solidify it for deposition of the next layer. Films with total thicknesses 150, 230 and 540 nm were prepared. An important precondition for formation of good films was a good wettability of substrate. In this case the solution covered the whole substrate without formation of big droplets, inhomogeneous drying of which can result in cracking (Figure 15) [69].

As the last step the films were annealed at high temperatures, chosen in the range 300–700 °C. The lower limit of temperature was selected to provide decomposition of organic precursors, burning out the excess of their carbon and provide defects relaxation in AZO lattice. The upper limit was set to avoid melting of used substrates.

It was revealed that the surface quality depends on the annealing temperature (Figure 16). Particularly surface becomes rough at 700 °C. Thus lower annealing temperatures should be used for obtaining smoother surfaces. Indeed more uniform surfaces were obtained, if annealing temperatures were kept in the range 400–500 °C.



**Figure 15.** An optical microscope image of shrunk and cracked AZO film.

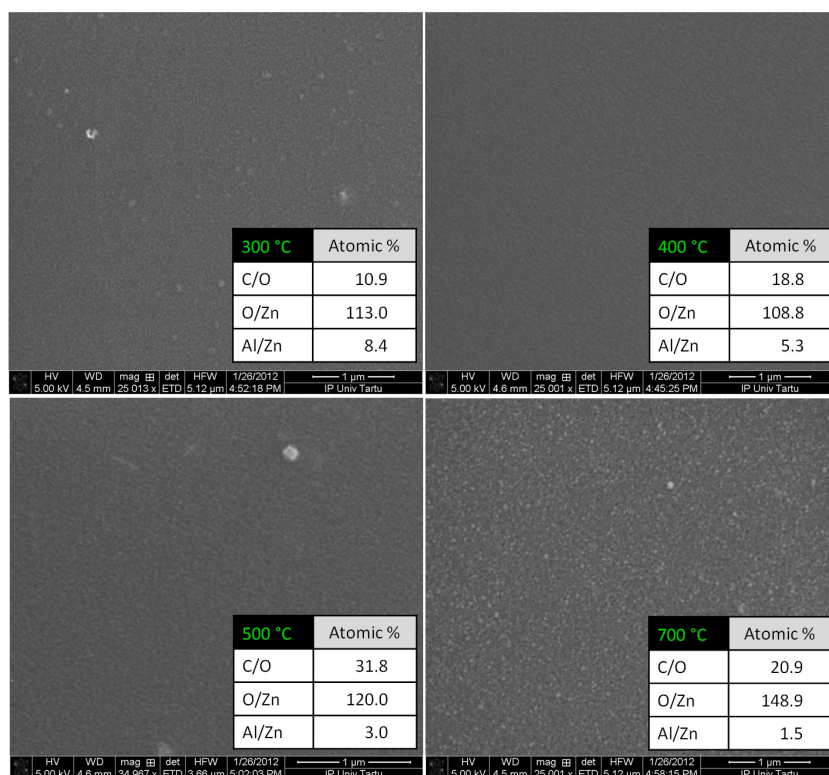


**Figure 16.** SEM images of AZO films after annealing at 300, 400, 500, 700 °C for 1 hour in air. Films have 5 layers. Route #1.

Films thickness decreases more than in 3 times after annealing (Figure 17, Table 2). It can be associated with major burning out of carbon. Indeed, the element analysis proves that C/Zn ratio decreases in more than 3 times after annealing (Figure 17), which correlates well with the decrease in film thickness. At the same time the ratio O/Zn was increased by 24 % as a consequence of annealing in oxygen-containing atmosphere.

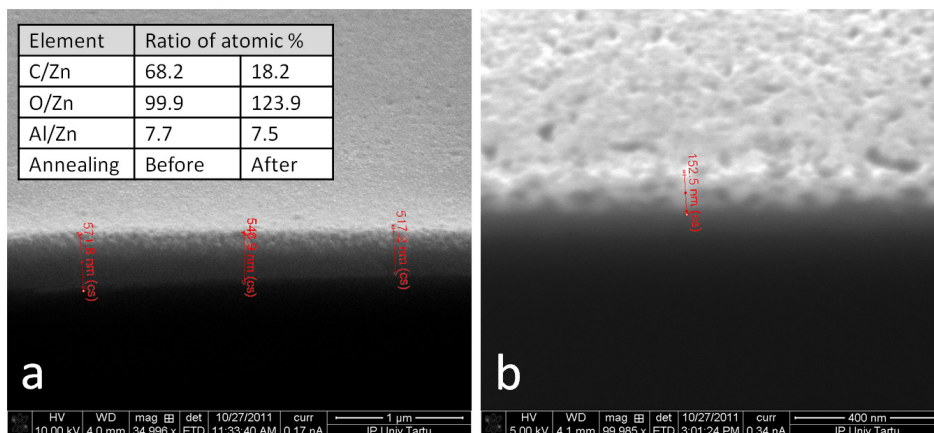


**Figure 17.** SEM images of AZO films before (a) and after (b) annealing. Route #1.

**Table 2.** Thicknesses of films obtained by route #1.

Annealing	Number of layers	Thickness, nm	Drying, °C	Annealing, °C
Before	1	150	260	-
	3	230	260	-
	5	540	260	-
After	5	150	260	500 Air

The resultant electrical conductivity of the prepared films depends on the Al content. Initial concentration of Al/Zn in the solution was taken around 1 atomic % as suggested by M. J. Alam and D. C. Cameron [30]. Sheet resistance of the samples annealed in air was in the range 50–100 MΩ/□, which is quite high. It can be caused by the excessive oxidation of films annealed in air. Indeed, changing the annealing atmosphere resulted in a decrease in sheet resistance. The lowest obtained value was 0.9 MΩ/□ for the samples annealed in Ar atmosphere at 400 °C (Table 3, route #1).

**Table 3.** Experimental results for ZnO films on glass substrates.

	№ layers	Drying, °C	Annealing, °C			$R_{\square}$ , $10^6 \Omega/\square$
			air	Ar	Ar:H <sub>2</sub>	
Route #1	5	260	300 1 h	-	-	50–100
			400 1 h	-	-	
			500 1 h	-	-	
			300 1 h	500 1h	-	80
			400 1 h			0.9
			500 1 h			2
Route #2	3	250	500 1 h	-	-	2
			-	500 10 min	-	0.12
			-	500 1h	-	0.030
			-	-	500 30min	0.004

Optical transmittance of the films was estimated in the spectral range 300–900 nm. It was measured for the deposited samples before and after annealing. Thinner films measured after annealing had higher transmittance, which is for visible light appeared over than 90 % (Figure 18).

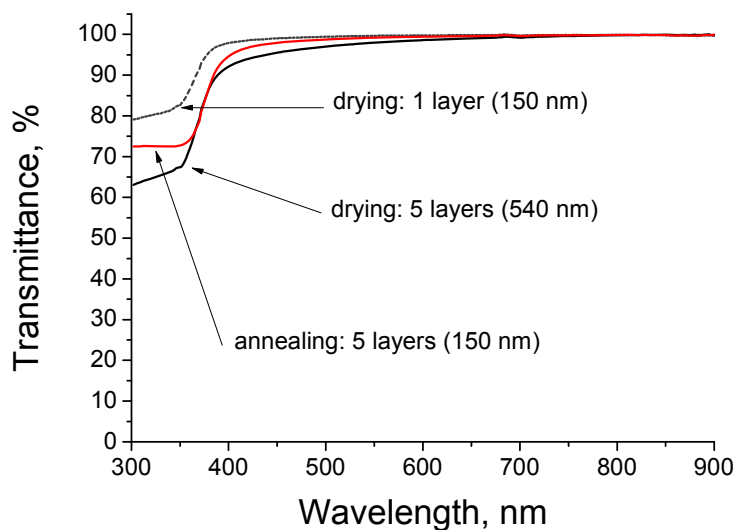


**Figure 18.** Transmittance of the AZO films with different thicknesses annealed in air. Route #1.

The summary of the parameters used in route #1 can be seen in Table 4.

**Table 4.** The summary of the parameters used in routes #1 and #2.

Material/Procedure	Route #1	Route #2
Zinc acetate dehydrate	0.8496 g	2.4815g
2-methoxyethanol	-	15 ml
Ethanol	60 ml	-
Ethanolamine [MEA]	-	0.65 ml
Aluminium nitrate nonahydrate	1at. %	0.5-3 at. %
Mixing (total time, temperature, speed)	180 min, 80 °C 300–1500 rpm	215 min, 73 °C 1000 rpm
Spin-coating (speed, solution amount, time, numbers of layers)	3000 rpm 170 µl 30 sec 1–5	3000 rpm 170 µl 30 sec 1–9
Drying (temperature, time)	260 °C, 10 min	200–400 °C, 1–10 min
Annealing (atmosphere, temperature and time, heating\cooling rate)	air, Ar 300–700 °C 60 min 2 °C per min	air, Ar, Ar:H <sub>2</sub> 500 °C 10–60 min 2 °C per min

The route #2 elaborated in course of the present work contains several changes for optimization of the conditions described in the route #1. Shelf life of the precursor solution was increased by substituting the solvent with 2-ethoxyethanol and adding ethanolamine as a complex agent. It permitted to avoid precipitation in the solution (Figure 19.a). The higher boiling temperature of 2-ethoxyethanol [86] in comparison with ethanol [87] resulted in slower evaporation. Additionally, it was possible to slow down the solution mixing speed.

Films spin-coated from the precursors prepared by route #2 (Table 4) had a uniform surface without particles (Figure 19.b). Thicker films can be prepared by multiple spin-coating and drying steps. It was revealed that the electrical resistivity of the films non-monotonously depends on the drying temperature (Figure 20.a). 250 °C was selected as the optimal drying temperature. This temperature is close to the melting point of the zinc acetate and corresponds to the minimal resistivity of the final films. Drying temperatures below 200 °C resulted in an essential decrease in the optical transparency of the films after aging.

Several additional tests were done for the determination of the optimal aging time for the prepared solution before spin-coating of the films and delays between drying and annealing and drying time. It was revealed that it is obligatory to stir the aged solution before deposition of the films. The drying time can be decreased from 10 to 1 minute without significant changes in the film

resistance. A delay in several days between the drying and annealing does not cause changes in the film properties.

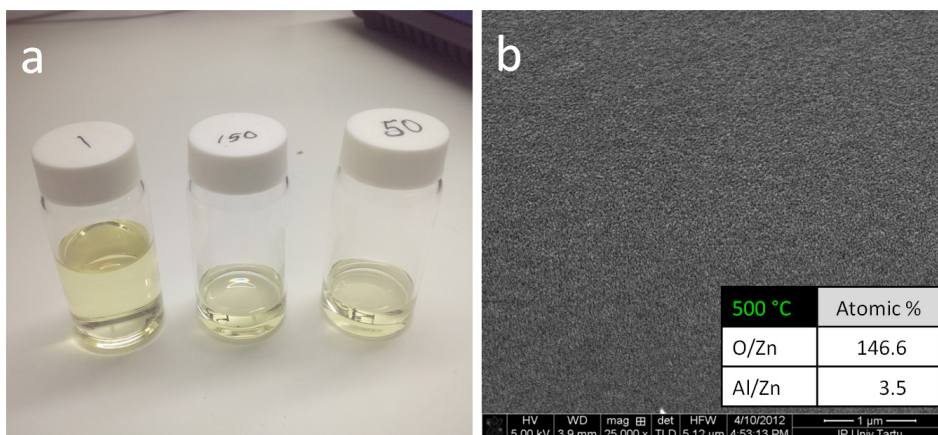


**Figure 19.** (a) Photos of capped bottles with solutions prepared by means of route #2: (mark 1) fresh solution; (marks 50 and 150) solutions aged for several months; (b) SEM image of AZO film prepared according to the route #2.

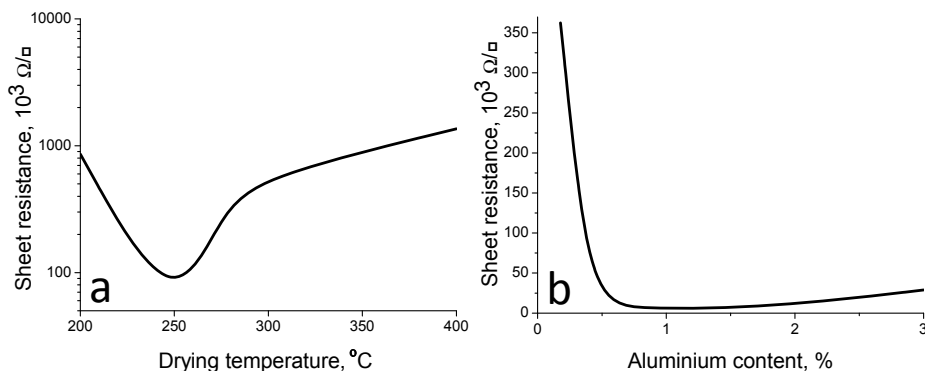


**Figure 20.** Sheet resistance of annealed AZO films as a function of (a) drying temperature and (b) concentration of aluminium dopant in the initial solution. Annealing in the cases (a) and (b) were done in different atmospheres. Route #2.

Annealing of samples was performed at 500 °C. This temperature was found to be most feasible for the formation of uniform sample's surface. The films prepared by means of route #2 and annealed in air had higher conductivity in comparison to the ones made according to the route #1. However, the achieved conductivity was not high enough. Changing the annealing atmosphere from air to Ar or Ar:H<sub>2</sub> was proposed to improve conductivity (Table 3). The annealing time was set dependently on the atmosphere. Annealing in the Ar:H<sub>2</sub> mixture required less time.

After achievement of acceptable resistivity values it was decided to investigate specially, how the sheet resistance depends on the concentration of the Al precursor. It was revealed that the sheet resistance of samples rapidly decreased with the increase of Al concentration, achieving a minimum near 1 % and then started to gradually grow (Figure 20.b). It was decided to use the Al concentrations corresponding to the minimum in the sheet resistance.

Experimentally it was revealed that thicker films had smaller resistance (Figure 21). It is in agreement with the theory where the resistance is inversely proportional to the thickness of the samples. In addition to this, the high resistance of very thin films can be caused by lattice mismatch between the ZnO:Al film and the substrate. Thicker layers have well-defined crystalline structure and lower amount of defects impeding conductivity.

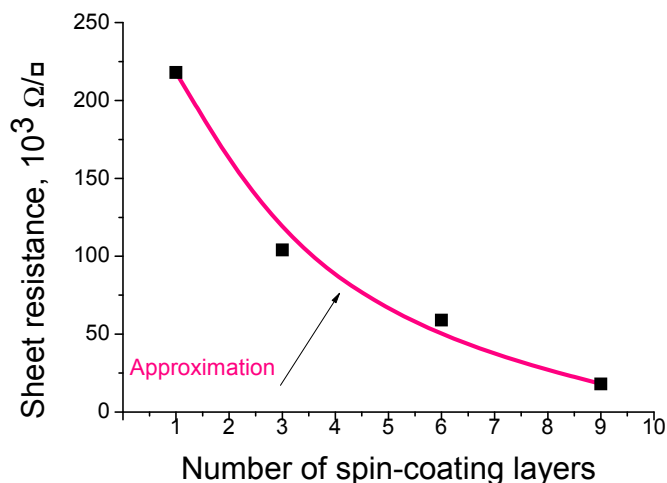


**Figure 21.** Sheet resistance of the AZO films vs. the number of spin-coating layers. Route #2.

Here it is important to pay attention to the notation related to the resistivity. Resistivity can be represented as the resistivity itself [88] or as the so called sheet resistance [89]. A special graph was elaborated for relating  $\rho$  and  $R_{\square}$  for samples of different thicknesses (Figure 22). It can be helpful for comparison of the resistivity values taken from different references.

Optical transmittance of the prepared films in the visible spectral range 400–900 nm was similar and had an average value near 95 % (Figure 23). Slight oscillations in the transmittance are connected with interference effect. It is more essential for thicker samples. Transmittance in the near ultraviolet spectral range is dependent on the film thickness also. The thicker was the film the lower was its transmittance. It was 70 % for the sample with only one layer of material and goes down to 5 % for the 9-layer film. Decrease in the light

transmittance in the ultraviolet range is caused by band-to-band light absorption in zinc oxide.

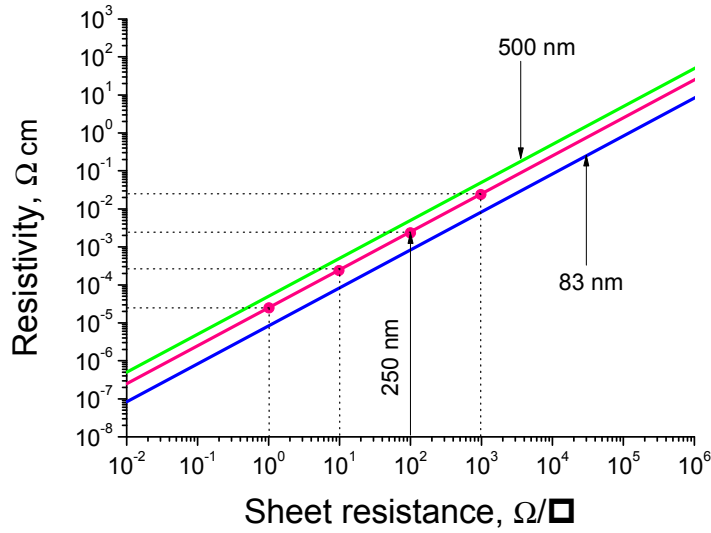


**Figure 22.** Dependence of  $\rho(R_{\square})$  for films with different thicknesses.

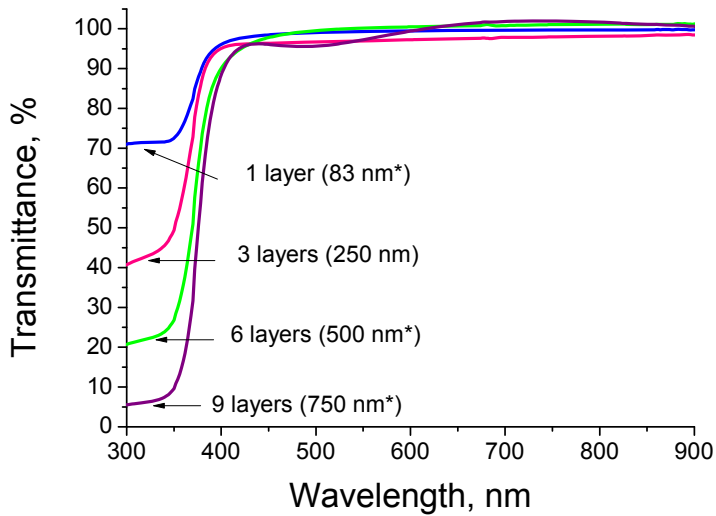


**Figure 23.** Light transmittance vs. wavelength of light for AZO films having different thicknesses. \*The thickness was estimated from the formula

$$\frac{250\text{nm}}{3} \times \text{amount\_of\_layers. Route \#2.}$$



The transmittance spectra were used for estimating the band-gap of AZO films. For this,  $(\alpha h\nu)^2$  was plotted as a function of  $h\nu$  (Figure 24). Each value of  $x$  and  $y$  were calculated by the formulas [90]:

$$x = h\nu = \frac{h c}{\lambda}; y = (\alpha h\nu)^2 = \left( \frac{-\ln(T)}{t} \frac{h c}{\lambda} \right)^2, \quad (4)$$

where  $t$  is film thickness [m],  $T$  is the transmittance in dimensionless units calculated from unity as from maximum level,  $\alpha$  is the absorption coefficient [1/m],  $h$  is Planck constant [eV·s],  $c$  is the speed of the light [m/s]. To obtain the bang-gap value, it was necessary to extrapolate the linear part of the plot in the corresponding near ultraviolet spectral range. Films with different numbers of layers had similar plot and the bang-gap was around 3.32 eV. This value correlates well with the literature data for ZnO [91].

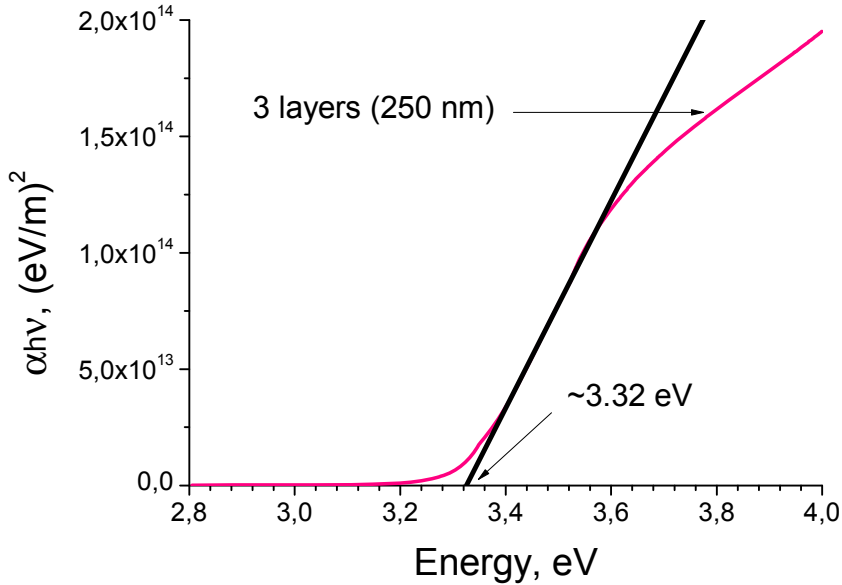


**Figure 24.** Band-gap estimation for 250 nm thick AZO film. Route #2.

The films were measured by X-ray diffractometer also (Figure 25). Generally the symmetric  $\theta/2\theta$  scan (XRD) gives information about the dominant plane orientations in the structure, whereas grazing incidence scan (GIXRD) determines the material itself via comparison with the known pattern. In our case XRD scan had one dominant peak near 002 and GIXRD had the same peaks as the calculated pattern of an ideal powder of ZnO. However, the absolute values were different. This indicates that the sample has an internal texture. On the basis on this we can conclude that our samples have a hexagonal

wurtzite structure such as ZnO and the atomic plane 001 is predominantly parallel to the plane of the sample.

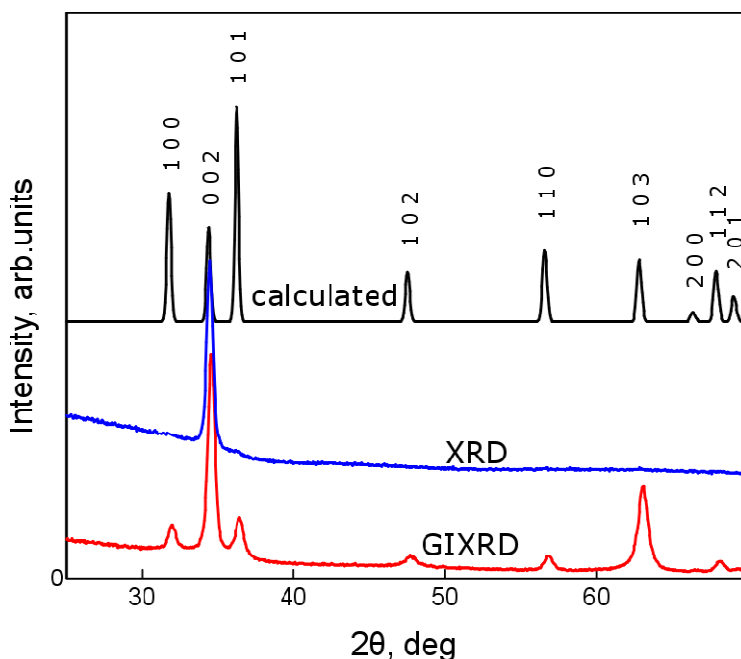


**Figure 25.** X-ray diffraction patterns of a AZO film: (blue) symmetric  $\theta/2\theta$  scan, (red) grazing incidence scan and (black) calculated pattern for ideal powder (structure data from ICSD collection code 67848). Miller indices are shown on top of the calculated peak positions. Route #2.

The summary of parameters used in route #2 are shown in Table 4.

## 4.2. AZO coatings made of fibers: preparation and properties

This section describes AZO coatings deposited by electrospinning method. In this case the structure is formed from a big amount of intersecting fibers. Several potential benefits can be achieved: some economy of material owing to the voids in the fiber mesh; these voids could also give an additional transparency to the whole structure; conductivity of sample through the intersecting fibers can be sufficiently high. Fiber based films were prepared by two routes, which gave thin and thick fibers, correspondingly. The structure and properties of these samples are discussed below.

As in section 4.1 the main precursors for preparation of the fibers can be zinc acetate dehydrate and aluminium nitrate nonahydrate. However, preparation of fibers requires higher viscosity of precursors. It was achieved by addition of polyvinylpyrrolidone to the solution of precursors. Initially the solution was loaded in syringe from which a small droplet was extruded. Then the droplet was elongated into the so-called Taylor cone, which was extracted from the droplet under the action of a high voltage. As a result, a continuous jet of material was formed between the electrodes [92–95]. Finally, the net of fibers was deposited by such way to the electrically charged substrate.

The conditions for preparation of thin and thick fibers were slightly different. They were named as route #1 and route #2, correspondingly. Specific details of these routes are shown in Table 5.

**Table 5.** Summary of the parameters used in route #1 and route #2 for preparation of fiber-based coatings.

Material/Procedure	Route #1	Route #2
Zinc acetate dehydrate	1 g	1 g
Deionized water	5 ml	2.5 ml
2-methoxyethanol	-	2.5 ml
Aluminium nitrate nonahydrate	1%	0–3 atomic %
Polyvinylpyrrolidone	0.5 g	0.87 g
Distance between the needle and samples	10 cm	15 cm
Electrospinning voltage	20 kV	14.5 kV
Feeding rate	0.12 $\mu\text{l}/\text{min}$	0.2 $\mu\text{l}/\text{min}$
Drying	-	in air at 150°C
Annealing	in air, at 100, 300, 400 or 450°C during 1 hour	in air or in vacuum at 360°C during 4 hours

The samples prepared by route #1 were annealed at different temperatures in the range 25–450 °C. It was revealed that an increase in temperature causes a decrease in fiber diameter (Figure 26). This decrease we associate with the burn out of fibers' components. Indeed, relative values of O/Zn before and after annealing at 450 °C were 2.1 and 2.9; relative values of C/Zn before and after annealing at 450 °C were 2.6 and 1.48. Consequently, the doped ZnO fibers had an increased amount of O and a decreased amount of C after annealing in air. This regularity is more pronounced at longer annealing times. The thinnest fibers were obtained at the temperature 450 °C (Table 6). As an extreme case, nanofibers can become very thin at high temperatures and therefore can be broken.

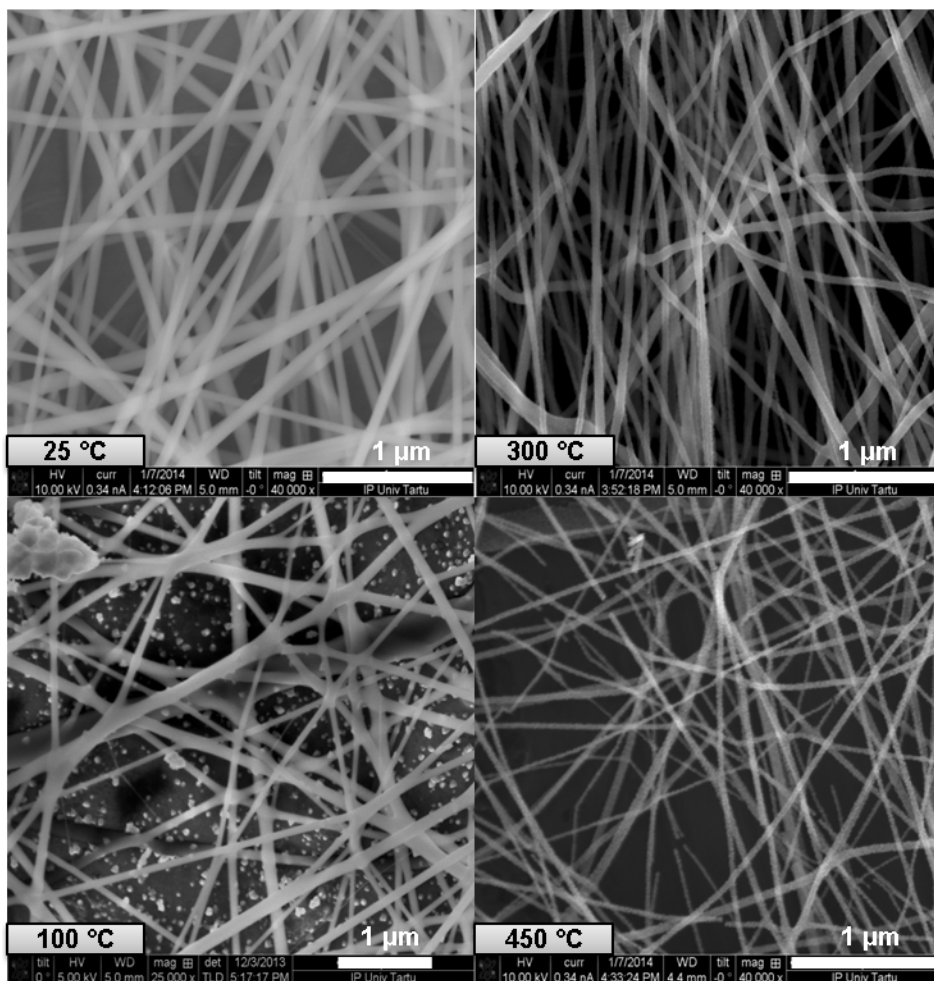


**Figure 26.** SEM images of AZO nanofibers annealed at different temperatures. Route #1.

**Table 6.** Influence of annealing temperature on the properties of the fibers prepared by route #1.

Max. annealing temperature °C during 60 min	Average fiber diameter, nm	Annealing procedure time, min	Heating and cooling rate, °C/min
-	95	-	-
100	95	180	1.5
300	57	427	1.5
450	40	627	1.5

Authors of Refs [92] and [94] met such difficulties connected with breaking, granulation and coalescence of thin fibers. In our case the same problem of fiber breaking appeared (Figure 26.d). To avoid breaking, the maximum temperature of annealing was decreased from 450 °C to 400 °C.

Granulation and coalescence of fibers were specially investigated and in our opinion they are connected with heating and cooling rates (Table 7). One can see that high heating rate led to deformation of nanofibers, loss of their uniformity and sticking of several thin fibers to thicker threads (Figure 27.a,b). However, application of a slow heating rate of 4.2 °C/min resulted in more uniform fibers with less coalescence (Figure 27.c,d). Thus, slow heating is important for formation of well-defined fibers, while the cooling rate is not so critical (Figure 27.c,d).

One can see that high heating rate results also in a granular structure of the fibers (Figure 27.a). Similar granulation of fibers was reported by Ding et al. [92]. Slow heating also solves this granulation problem and results in more smooth fibers (Figure 27.c,d).

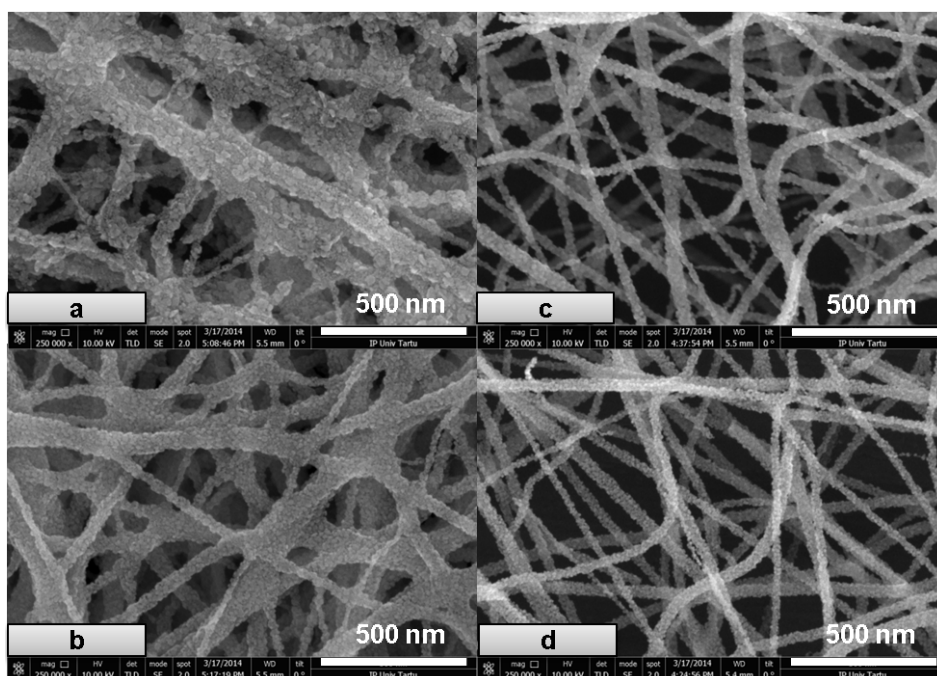


**Figure 27.** SEM images of AZO nanofibers annealed at different heating/cooling rates: (a) heating rate 12.5 °C/min, cooling rate 75 °C/min; (b) heating rate 12.5 °C/min, cooling rate 12.5 °C/min; (c) heating rate 4.2 °C/min, cooling rate 75 °C/min; (d) heating rate 4.2 °C/min, cooling rate 4.2 °C/min. Route #1.

**Table 7.** Influence of annealing on the properties of the fibers prepared by route #1.

Sample	Max. annealing temperature °C during 60 min	Average diameter of fiber, nm	Annealing procedure time, min	Heating rate, °C/min	Cooling rate, °C/min
a	400	84	95	12.5	75.0
b	400	54	120	12.5	12.5
c	400	42	155	4.2	75.0
d	400	31	240	4.2	4.2

It was uncovered that the samples prepared according to the route #1 were very sensitive to high humidity. If humidity during fiber deposition was 60–70 %, the jet of solution did not sufficiently evaporate during the electro-spinning process. It resulted in a change in viscosity and finally flabby fibers (Figure 28). In order to improve the structure of the fibers and make them less sensitive to humidity, route #1 was modified to route #2. Namely, 2-methoxyethanol was added to the initial solution. Concentration of polyvinylpyrrolidone was also increased. Additionally, the samples were dried before annealing.

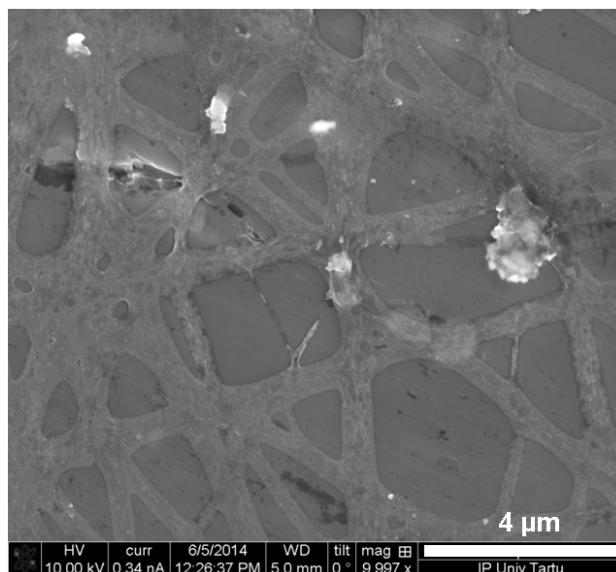


**Figure 28.** SEM images of AZO “nanofibers” produced at humidity 66 %. Route #1.

As in the case of spin-coated films (section 4.1) we slightly varied the concentration of aluminium in the case of route #2. As it was mentioned by S. Yun at al. [94], increasing of Al content can cause a non-uniform structure of the resulting fibers. In our case the fibers with larger Al/Zn ratio had a uniform structure (Figure 29) and their average diameter was smaller (Table 8). It can be

that aluminium increases polarizability of the solution jet, which results in better exhaustion of thinner fibers [96].

**Table 8.** Dependence of fibers' diameter on the concentration of aluminium and annealing atmosphere. Route #2.

Al/Zn, atomic %	Average fiber diameter, nm	
	annealing in air	annealing in vacuum
0.0	140	157
0.5	135	159
1.0	138	157
1.5	130	137
2.0	116	111
3.0	104	108

Thickness of the fibers was also influenced by the level of burning out of their constituents. Thus, fibers annealed in vacuum were slightly thicker compared to those annealed in air (Table 8). It can be explained by increased amount of carbon in them. For example, the C/Zn ratio was 4.49 and 0.72 for the samples annealed in vacuum and in air, correspondingly.

There were small granulations on the surface of the fibers annealed in air (Figure 30). However, the surface of the fibers annealed in vacuum looked smoother.

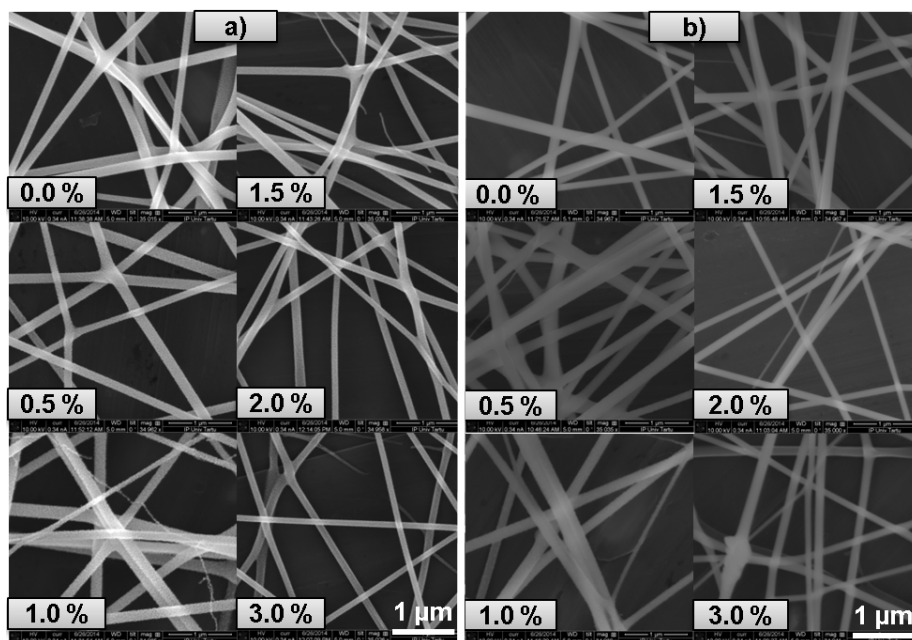


**Figure 29.** SEM images of AZO nanofibers annealed in: a) air and b) vacuum. Concentration of Al is represented in atomic %. Route #2.

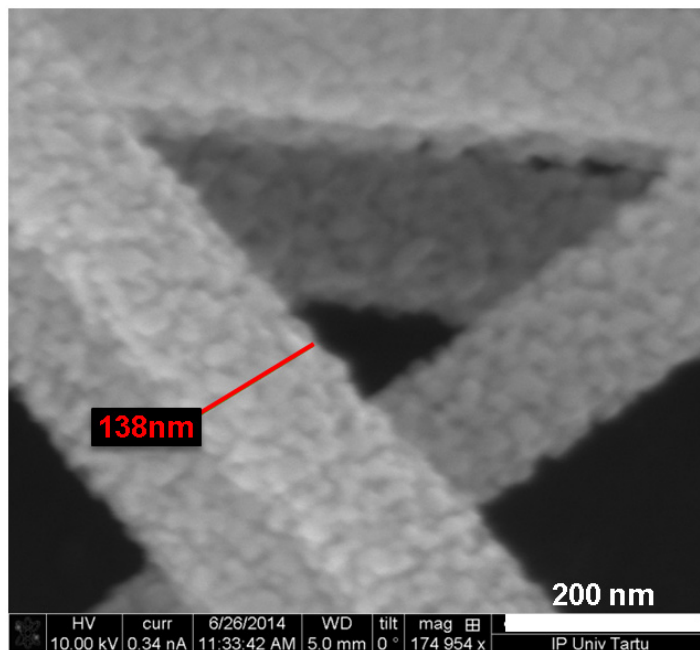


**Figure 30.** SEM images AZO nanofibers annealed in air, concentration of Al is 1 %. Route #2.

Fiber based films had optical transmittance above 90 % in the visible spectral range (Figure 31). The transmittance in the near ultraviolet spectral range was still high, whereas for the spin-coated films it was significantly dependent on film thickness (Figure 23). We can explain these phenomena by the presence of voids between the nanofibers, where the transmittance was mostly determined by the glass substrate.

Transmittance of the samples annealed in air was slightly higher than those annealed in vacuum. Since the fibers annealed in air and vacuum had approximately the same diameter (Table 8), we suggest that the higher transmittance is caused by higher fibers' porosity. It was formed by burning out of a significant part of the organic components during the annealing in air.

Sheet resistance of fiber-based samples was in the range of hundreds of  $M\Omega/\square$ , which is higher than that of the spin-coated films (section 4.1). It can be connected with bigger amount of defects in the fibers. Another reason of high sheet resistance can be that the amount of conductive channels made by intersecting fibers is not sufficiently high.



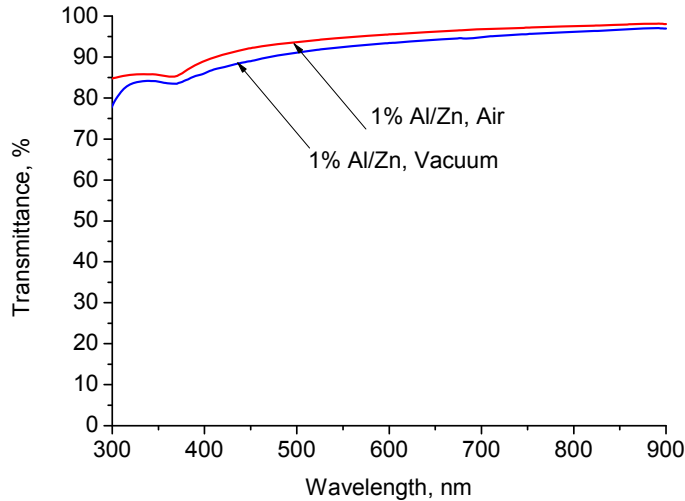


**Figure 31.** Transmittance spectra of AZO films annealed in air (1) and vacuum (2).

### 4.3. Optical performance of AZO films used as a part of layered coatings and liquid crystal indicators

Here it is demonstrated that AZO films in combination with other optical and electro-optical layers can be used for the control of spectral shape and propagation direction of fluorescent light (section 4.3.1). Particularly, combination of AZO layer with gold nanofilm can be prospective for driving fluorescence intensity and direction in the reflective type fluorescent displays [97–99], and optical fluorescent sensors working in reverse Kretschmann mode [100].

Sufficiently good transparency and electric conductivity of prepared layers make possible also their usage in liquid crystal electro-optical indicators (section 4.3.2). To the best of our knowledge, the usage of sol-gel prepared AZO films in such structures have not been tested before. Therefore the revealed optical effects are interesting both from the scientific and applied points of view.

#### 4.3.1. AZO-gold layer for the resonant control of fluorescence

As it was pointed out before, the prepared AZO films are transparent for the visible light. However, they strongly absorb the light in the ultraviolet spectral range. This absorption can stimulate both transition of electrons from the valence to the conduction band and also trapping of electrons at the lattice defects, which are energetically situated inside the ZnO bandgap. Radiative relaxation of such electrons can cause a weak, but detectable fluorescence [101] of the samples in the broad spectral range from 400 to 700 nm (Figure 32).

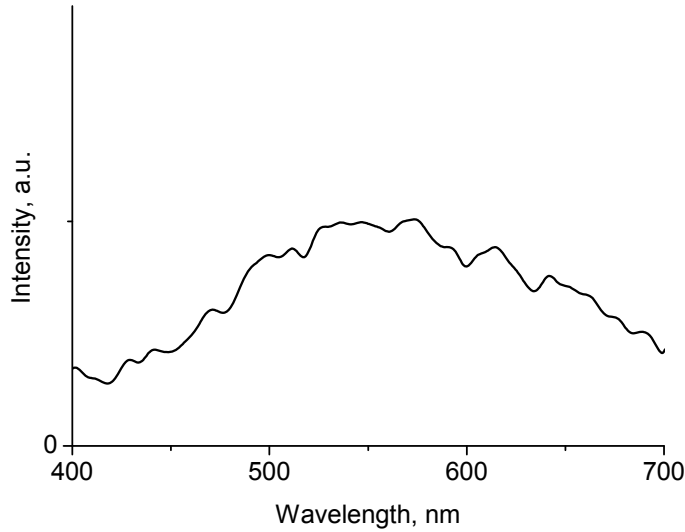


**Figure 32.** The fluorescence emission spectrum of AZO film deposited on a glass substrate.

Below it is demonstrated that for the 2-layer coating, which includes AZO and gold layers, it is possible to vary the spectral shape and the intensity of the fluorescence by changing angular position of the detector.

Bringing light into the film can be organized through a semicylindrical prism, which is in optical contact with the film (Figure 33). Such method is frequently used for coupling light into planar optical waveguides [102]. Light can follow the waveguide or be reflected outside of it. Here the third possibility is investigated, when the light can be partially transformed into the special kind of surface wave. Light beams, which are reflected or excited near the AZO-gold interface on the side of prism, can induce resonance with light oscillations of surface electrons in the gold layer. The electric field of these oscillations, which are also called surface plasmon-polaritons, can influence the fluorescence process by supporting it for certain spectral ranges, spatial directions and polarizations.

The surface wave appears in the case when the light is detected through the prism attached to the AZO-gold interface. Detector is placed in the range of angles, which satisfy the condition of the total internal reflection. Reverse propagation of light beams does not change the optical laws of light propagation. Therefore the conditions for coupling of light with surface waves should be identical in spite of fluorescent or reflection nature of the light beam. Therefore it was decided initially to investigate the reflected light in the mentioned AZO-gold structure and compare it with fluorescence.

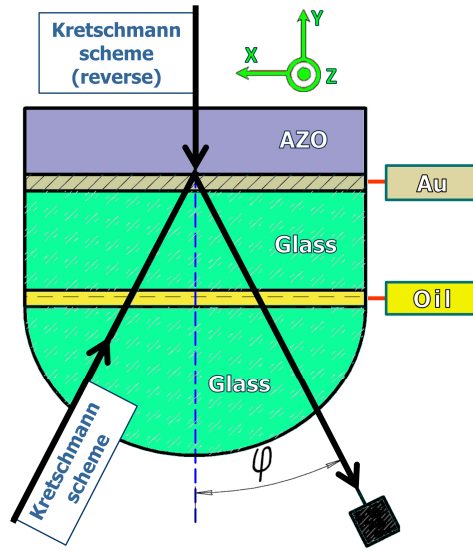


**Figure 33.** Introduction of light into the film by means of a prism: Kretschmann [84] scheme is that, in which the light comes through the prism; reverse Kretschmann scheme is that, in which the light is absorbed from the side of film and can be transformed to fluorescence detected at an angle  $\varphi$ .

The laser light source with 532 nm wavelength was specially selected by such a way to be coincident with the maximum of the fluorescence of AZO films. It gave a possibility for further comparison of the reflected and fluorescent light in the same spectral range.

Intensity of the reflected light demonstrated dips if detector scanned certain detection angles (Figure 34). One can see that the dip for the p-polarized light is situated at  $\sim 42^\circ$  (Figure 34.a) and the dip for s-polarized light is at  $\sim 55^\circ$  (Figure 34.b). The dips have not only different angular position, but also different shape and half width. Optically it means different conditions for the interference of s- and p-polarized light incident on the AZO-gold interface. This interference can be described by generalized Fresnel equations, in which the metal is considered as a medium having a complex permittivity with real part and imaginary part [103]. Since the practical use of these equations is most convenient in the matrix form, the method is called the transfer matrix method in the literature [104,105].

Here calculations of the light reflection in case of p-polarized and s-polarized light are represented. Both for AZO and for the gold layers one can write the equations connecting their complex refractive indices  $n_j$  depending on the wavelength of light  $\lambda$  and thicknesses of layers  $d_j$ . This approach can be generalized on the several layers, each of which has own number  $j$ , starting from the layer number 1, which is the prism in our case.

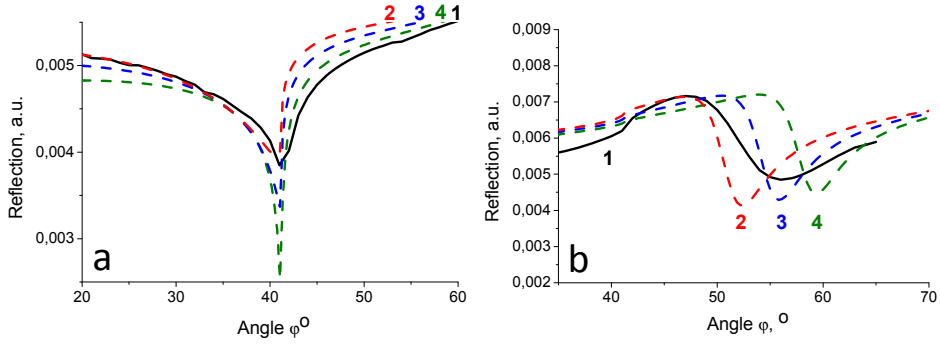


**Figure 34.** Experimental (solid, 1) and theoretical (dashed, 2–4) curves for reflection of p-polarized (a) and s-polarized (b). Thicknesses of AZO films are taken as: (2) 230 nm, (3) 240 nm, (4) 250 nm.

Therefore we keep the notation  $j$  remembering that in our case  $j=1, 2, 3$  and layer 1 is the prism and layers 2 and 3 are gold and AZO, correspondingly:

$$\beta_j = \frac{2\pi d_j}{\lambda} \sqrt{n_j^2 - n_1^2 \sin^2 \varphi}, \quad (5)$$

where  $\varphi$  is the detection angle taken on the side of prism from the normal to the film surface,

$$p_j = \sqrt{n_j^2 - n_1^2 \sin^2 \varphi}, \quad j = 2, 3, \quad (6)$$

$$M_j = \begin{pmatrix} \cos \beta_j & \frac{-i \sin \beta_j}{p_j} \\ -ip_j \sin \beta_j & \cos \beta_j \end{pmatrix}, \text{ for s-polarized light} \quad (7)$$

or

$$M_j = \begin{pmatrix} \cos \beta_j & \frac{-in_j^2 \sin \beta_j}{p_j} \\ \frac{-ip_j \sin \beta_j}{n_j^2} & \cos \beta_j \end{pmatrix}, \text{ for p-polarized light.} \quad (8)$$

The matrix characterizing light reflection can be obtained as a result of multiplication of matrices of corresponding  $j$  layers:

$$M = M_2 \times M_3 \times M_4 \times \dots \times M_N \text{ in our case } M = M_2 \times M_3. \quad (9)$$

The elements of the resulting square matrix  $M$  are used for the calculation of the reflection coefficient and intensity of reflected light  $R(\theta)$ :

$$M = \begin{pmatrix} m_{11} & m_{12} \\ m_{21} & m_{22} \end{pmatrix}, \quad (10)$$

$$r = \frac{(m_{11} + m_{12}p_N) - (m_{21} + m_{22}p_N)}{(m_{11} + m_{12}p_N) + (m_{21} + m_{22}p_N)}, \quad (11)$$

$$R(\theta) = |r|^2. \quad (12)$$

Calculations were carried out for  $n_1 = 1.519$ ,  $n_2(532) = 0.544 + 2.14i$ ,  $d_2 = 50$  nm,  $n_3 = 2.03$  and a set of  $d_3$  thicknesses 230 nm, 240 nm, 250 nm (Figure 34, curves 2–4). We took  $d_3$  thickness as 240 nm, which better corresponds to the experimental curves (Figure 34, curves 3).

The dip in the intensity of the reflected light is caused by the excitation of the waveguiding modes in the structure. In case of p-polarization also excitation of surface plasmon polaritons is possible. The electrical field distribution inside the gold-AZO structure was calculated and plotted in Figure 35. Detection angles  $\varphi$  corresponding to the dips in the reflection for p- and s-polarized light were used in the calculation.

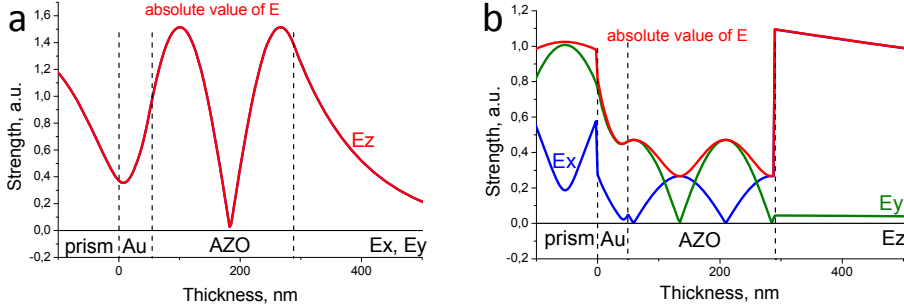


**Figure 35.** Calculated distribution of electric field inside the layered structure for (a) s-polarized reflection,  $\lambda = 532$  nm,  $\varphi = 55^\circ$ ; (b) p-polarized reflection,  $\lambda = 532$  nm,  $\varphi = 42^\circ$ .

As surface plasmon polaritons could be only excited by a p-polarized light, the distribution of the electrical field z-component  $E_z$  for s-polarized light (Figure 35.a) can be associated only with the waveguiding of the light inside the AZO film, but not with the plasmon-polariton surface wave. On the other hand, in case of p-polarization (Figure 33.b) it is possible to excite both ordinary waveguiding modes and surface plasmon polaritons. We can judge that there is a kind of a hybrid distribution of the electric field near the gold-AZO interface, which can be mainly associated with waveguiding and partially associated with surface plasmon-polaritons. Such kind of hybrid modes are described also in the literature [106]. It was shown earlier for the film-gold interface that plasmonic influence on light reflection can be more essential if the thickness of films deposited on gold is less than 50 nm [107,108].

The angular distribution of AZO fluorescence has also a non-monotonic behaviour. The angular positions of extreme points for fluorescence are the same as for the reflection of light at the same wavelengths. As was mentioned above, it is resulted from the possibility of the reverse way for the light beams.

However, fluorescence demonstrates intensity maxima at angles where the reflection had minima (Figure 36). It is a non-trivial behaviour of light and can be explained by the influence of the mentioned waveguide and hybrid modes on the fluorescence process.

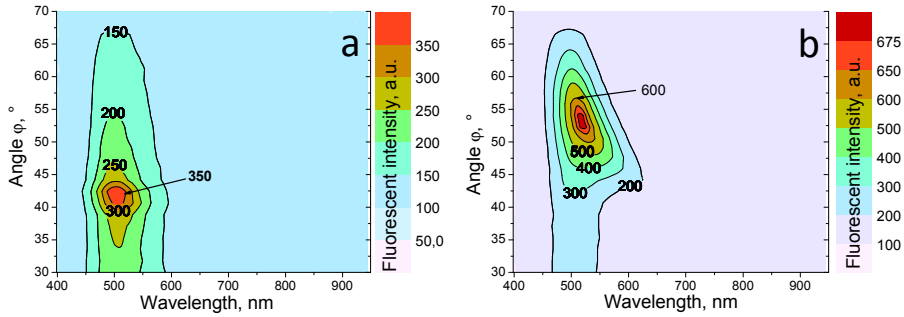


**Figure 36.** The diagram of p-polarized (a) and s-polarized (b) fluorescence from an AZO film deposited on a gilded glass and detected through the prism at different angles  $\varphi$ .

When the fluorescent centers are present near the metal-dielectric interface, there is a competition between the direction of energy to plasmon/waveguide modes or to fluorescence. If the fluorescence process is beneficial, plasmonic dip in the angular dependence of intensity becomes hidden [58]. When the contribution of plasmons becomes comparable to the fluorescence, the angular maximum in the fluorescence disappears so that the intensity of light will not change with the angle. If the contribution of plasmons prevails over the fluorescence, it becomes possible to detect the dip in the angular characteristic of the fluorescence [57]. It appears in case when most of the energy of the excited fluorescent centres is transferred to plasmons.

In our case the coupling of waveguide mode with fluorescence allows to re-shape the fluorescence spectrum by the selection of detection angle. It follows just from the asymmetric view of the intensity diagram for s-polarized light (Figure 36.b) in comparison to the diagram for the p-polarized light (Figure 36.a). For example, the maximum of the fluorescence at the 525 nm detected for the angle 53.8° is shifted to 537 nm, if the detection angle is set to 52.5°. Such re-shaping of fluorescence spectrum can be considered as a simpler alternative to the re-shaping of fluorescence in photonic crystals [109].

#### 4.3.2. Use of AZO electrodes in the liquid crystal cell

The AZO films described in section 4.1 were tested as conductive layers of the liquid crystal indicators. The prepared liquid crystal cell was transparent in crossed polarizers, which implies that the electric vector of linearly polarized light was rotated by 90° inside the twisted liquid crystal layer (Figure 37.a).

Visual examination was made for the dark appearance of sample in parallel polarizers providing a better visualization of possible defects in the liquid crystal alignment (Figure 37.b).

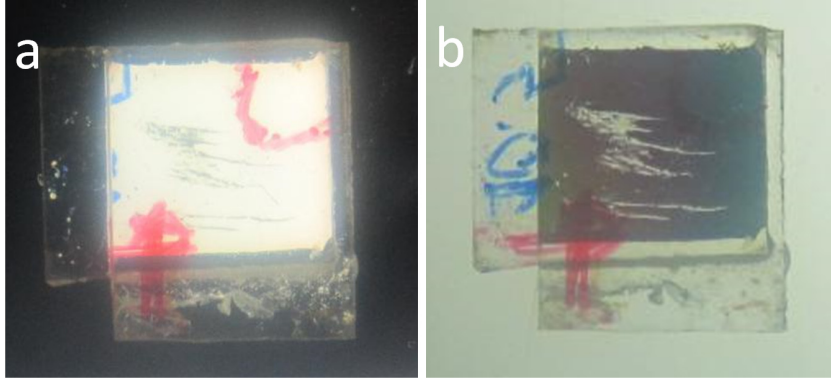


**Figure 37.** Macroscopic image of prepared twisted-nematic cell. Transmitted light viewed through (a) crossed polarizers and (b) parallel polarizers. The crossed red arrows show the rubbing directions of the substrates coinciding with the axes of crossed polarizers (a). The red mark at the top right corner corresponds to the area with the most homogeneous liquid crystal alignment.

White stripes on the black background (Figure 37) correspond to the defects in the liquid crystal orientation. Such defects are caused by imperfections in laboratory techniques for deposition and rubbing of orienting polymer layer or some microroughness of the underlying AZO layer. However, the sample was sufficiently good for the measurements of its transmittance in the course of switching.

The switching of the prepared liquid crystal cell placed between crossed polarizers was investigated by observing the changes of its light transmittance under the applied electric voltage (Figure 38).

The usual equation for the threshold voltage needed for the switching of cell includes parameters of the liquid crystal [110]:

$$U = \pi \sqrt{\frac{K_{11} + \frac{1}{4}(K_{33} - 2K_{22})}{\epsilon_0 \Delta \epsilon}} \quad (13)$$

where  $K_{11}$ ,  $K_{22}$ ,  $K_{33}$  are the coefficients of elasticity of the liquid crystal,  $\Delta \epsilon$  is the dielectric anisotropy of the liquid crystal.

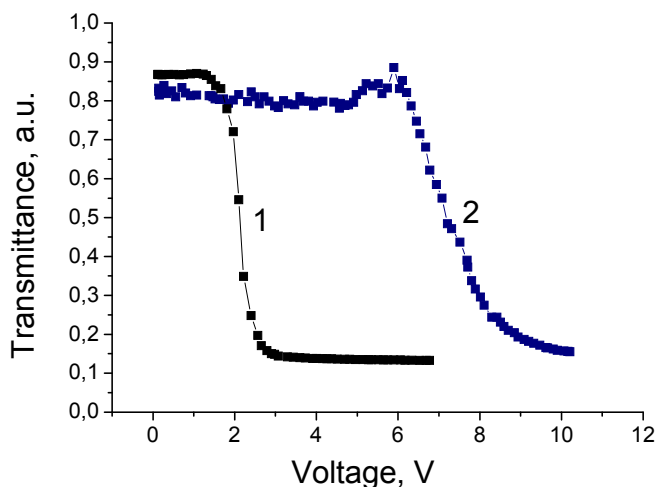


**Figure 38.** Transmittance vs. voltage for the twisted liquid crystal cells based on ITO (1) and AZO (2).

Substituting these parameters of the liquid crystal ZLI4792 into the equation, one can obtain the threshold voltage 1.76 V, which is close to the experimental value obtained for the sample with ITO as a conductive electrode (Figure 38, curve 1). However, the threshold voltage is 3 times higher for the sample based on the AZO film. It is because of a lower conductance of the AZO electrodes. Such lower conductance is caused mainly by lower charge concentration in the AZO film, which implies application of higher external voltage for reorienting liquid crystal molecules. This example testifies that traditional equations for electro-optical switching of liquid crystals need some adaptation for the cases of electrodes with different conductivities. Despite of higher value of driving voltage we demonstrated an acceptable electro-optical behaviour of the liquid crystal cell based on the AZO films prepared by sol-gel method. A small spike near 6 V in curve 2, Figure 38 is connected with the higher pretilt angle of liquid crystal molecules in case (2) in comparison with case (1).



## CONCLUSIONS

### Processing and characterization of transparent electrode materials

Thin Al-doped ZnO (AZO) films can be considered as alternative to the indium tin oxide films for transparent electrode applications. AZO consists of cheap and abundant chemical elements compared to indium based materials. In this PhD work it was studied how the tiny changes in the chemical composition of initial solutions and conditions of further treatment influence the structure, electrical and optical properties of the resulting AZO films. Sol-gel routes were elaborated in details in the course of this work and such preparation conditions as humidity, temperature and atmosphere of heat treatment were taken into account. Sol-gel method is accentuated here as it is easier, more accessible and relatively inexpensive in comparison with such complex techniques as atomic layer deposition or magnetron sputtering.

An essential attention in this work was devoted to the investigation of the prepared AZO films as components of electro-optical layered structures. It is described how the intensity, polarization and spectral shape of defect-related fluorescence can be controlled for the films deposited on the thin gold layers. Electro-optical behaviour of liquid crystal indicators in which prepared films are used as transparent conductive electrodes is investigated. The main results and novelty of the work are summarized as follows:

- Continuous AZO films were prepared from sol-gel precursors by means of spin-coating and subsequent annealing. The thickness of the final coatings was in the range of several hundred nanometers depending of the amount of spin-coating cycles. It was revealed that ~1 % of aluminium in the initial solution provided the lowest sheet resistance for the prepared samples in the range of several  $\text{k}\Omega/\square$ . The lowest resistance was achieved for the samples annealed in  $\text{Ar:H}_2$  atmosphere preventing unwanted oxidation of the samples.
- Fiber-based AZO coatings were made by electrospinning method, where fibers with nanosized cross-sections were developed from extruded droplets of sol-gel solution under the action of electrical field. Thus developed approach can be prospective for preparation of fibers for electro-optic applications. It was important to keep a moderate heating rate ~1–4 °C per minute during annealing of samples in order to avoid granulation and coalescence of fibers. Comparatively high sheet resistance of the samples can be explained by a low amount of conductive channels made by intersecting fibers.
- Moderate fluorescence associated with lattice defects in AZO films was registered. The intensity and polarization of the emission could be controlled if the samples were deposited on a gold-coated glass substrate. Directional

resonant fluorescence was detected at the same angles at which attenuated internal reflection from the AZO–gold interface occurred. Selection of proper detection angles allowed redistribution of fluorescence intensity and polarization for the wavelengths of fluorescent light, for which effective coupling with hybrid plasmon-waveguide or pure waveguide modes is realized.

- It was demonstrated that the prepared continuous AZO films can be used as a conductive layers in the liquid crystal indicators. Particularly satisfactory quality was achieved in the orientation of the twisted-nematic type liquid crystals. The transparency of prepared indicator could be changed 8 times by the application of driving voltage  $\sim 6$  V.

## SUMMARY IN ESTONIAN

### Läbipaistvate elektroodmaterjalide väljatöötlus ja karakterisatsioon

Alumiiniumiga dopeeritud ZnO (AZO) kiled pakuvad alternatiivi indium-tina-oksiidile läbipaistvaid elektroode nõudvates rakendustes. Võrreldes indiumipõhiste materjalidega koosneb AZO odavatest ja levinud keemilistest elementidest. Käesoleva doktoritöö raames uuriti kuidas väikesed muutused alglahuste keemilises koostises ja järeltöötamise tingimustes mõjutavad saadud AZO kilede struktuuri, elektrilisi ja optilisi omadusi. Sool-geel protsessi viimistleti detailselt võttes arvesse niiskust, temperatuuri ja lõõmutusatmosfääri. Käesolevas töös rõhuetasetus on sool-geel meetodil, mis on võrdlemisi lihtne, kättesaadav ja odav võrreldes keerukate sünteesimeetoditega nagu aatomkihtsadestamine ja magnetron-pihustamine.

Peamine tähelepanu selles töö on koondatud AZO kilede kui elektro-optiliste struktuuride ühe võimaliku komponendi uurimisele. Kirjeldatakse õhukesele kulla kilele sadestatud AZO kihtide fluorestsentsi intensiivsuse, polarisatsiooni ja spektri kuju kontrollimist. Uuriti vedelkristallindikaatorite toimimist kus sünteesitud kiled toimisid läbipaistvate elektroodidena. Töö peamised tulemused ja uudsus on järgmised:

- AZO kiled valmistati sool-geel meetodil vurr-katmisega. Pärast lõõmutamist olid saadud kilede paksused mõnesaja nanomeetri suurusjärgus sõltuvalt vurrkatmistüklite arvust. 1%-lise alumiiniumi sisalduse korral alglahuses saavutati madalaim kilede pindtakistus paari  $k\Omega/\square$  vahemikus. Madalam takistus saavutati kui proove lõõmutati  $Ar:H_2$  atmosfääris, mis pärssis materjali soovimatut oksüdeerumist.
- Fiibripõhised AZO katted valmistati elektroketruse meetodil, kus nanomõõtmelise diameetriga fiibrid tõmmati sool-geel lahuse tilkadest elektrivälja toimetel. Arendatud meetod on perspektiivne katete valmistamiseks elektro-optiliste rakenduste jaoks. Oluliseks osutus mõõduka kuumutuskiiruse ( $\sim 1-4$  °C/min) säilitamine proovide lõõmutamisel vältimaks fiibrite granuleerumist ja kokkukleepumist. Võrdlemisi saadud proovide kõrget kilede pindtakistus võib selgitada vähesel hulgal juhtivate kontaktide tekkinemisega fiibrite vahel.
- Registreeriti mõõduka tugevuse fluorestsentsi, mis on seotud defektidega AZO kiledes. Selle emissiooni intensiivsust ja polarisatsiooni õnnestus kontrollida kui kile sadestati õhukese kullakihi kaetud klassalusele. Suunatud resonantset fluorestsentsi detekteeriti sellistes suundades, kus leidis aset mittetäielik sisepeegeldus AZO-kulla piirpinnal. Detektsiooni suuna sobiv valik lubas moduleerida fluorestsentsi intensiivsust ja polarisatsiooni

nendel lainepikkustel, mille puhul tekkis efektiivne sidestus lainejuhi moodide või lainejuhi-plasmoni hübriidmoodidega.

- Demonstreeriti et saadud AZO kilesid on võimalik kasutada elektrit juhtivate kihtidena vedelkristallindikaatorites. Iseäranis rahuldav kvaliteet saavutati väänatud nemaatiku tüüpi vedelkristallide orienteerimisel. Valmistatud indikaatorite läbipaistvust õnnestus muuta 8 korda rakendades pinget  $\sim 6$  V.

## ACKNOWLEDGEMENTS

I am very grateful to my supervisors Prof. A.E. Romanov and Dr. L. Dolgov for their assistance and encouragement to finish this thesis successfully. Special thanks to the head of laboratory of laser spectroscopy I. Sildos for providing all necessary equipment to complete my work successfully. I would like to say thank all co-authors who took part in this collaboration work: I. Kink, A. Loot, V. Kiisk, S. Lange and others. Additional special thanks to L. Dorogin, J. Šulga, S. Vlassov for their inspiration, R. Saar for help with SEM measurements, H. Mändar for XRD measurements. I also kindly acknowledge the technical support in examination of AZO films in liquid crystal indicators “Department of molecular and liquid crystals, Institute of Physics, NAS of Ukraine” and personally the scientific associate R. Kravchuk and Dr. O. Yaroshchuk.

I would like to thank my relatives and friends for their support.

I am thankful for the financial support by European Social Fund’s Doctoral Studies and Internationalization Program DoRa, “Low-dimensional structures and their applications” SF0180058s07, “Structure sensitive interaction mechanisms in functional materials at nanoscale” IUT2-25, ERDF (Centre of Excellence “Mesosystems: Theory and Applications”, TK114), ETF grant “Processing, characterization, and modeling of nanoparticles-reinforced multiscale composites” 8420, Estonian Nanotechnology Competence Centre (EU29996), ERDF “TRIBOFILM” 3.2.1101.12-0028, “IRGLASS” 3.2.1101.12-0027, “Nano-Com” 3.2.1101.12-0010, NATO SPS project grant NUKR.SFPP984702 and the European Union funded by European Regional Development Fund.

## REFERENCES

- [1] Global Industry Analysts, Inc., Online: [http://www.strategyr.com/MarketResearch/Sol\\_Gel\\_Products\\_Market\\_Trends.asp](http://www.strategyr.com/MarketResearch/Sol_Gel_Products_Market_Trends.asp); last accessed 2017\_05\_20
- [2] E. Fortunato, D. Ginley, H. Hosono, D. C. Paine, Transparent Conducting Oxides for Photovoltaics, *MRS Bull.* (2007), 32, 242–247; (doi:10.1557/mrs2007.29).
- [3] H. Liu, V. Avrutin, N. Izyumskaya, Ü. Özgür, H. Morkoç, Transparent conducting oxides for electrode applications in light emitting and absorbing devices, *Superlattice Microst.* (2010), 48, 458–484; (doi:10.1016/j.spmi.2010.08.011).
- [4] J. Siegel, O. Lyutakov, V. Rybka, Z. Kolská, V. Švorčík, Properties of gold nanostructures sputtered on glass, *Nanoscale Res. Lett.* (2011) 6, 96; (doi:10.1186/1556-276X-6-96).
- [5] M. Avrekh, B. M. Thibadeau, O. R. Monteiro, I. G. Brown, Transparent, conducting, metallic thin films, *Rev. Sci. Instrum.* (1999) 70, 4328; (doi:10.1063/1.1150075).
- [6] D. S. Ginley, Ed., *Handbook of Transparent Conductors*. Springer (2011); (doi:10.1007/978-1-4419-1638-9).
- [7] F. Bonaccorso, Z. Sun, T. Hasan, A. C. Ferrari, Graphene photonics and optoelectronics, *Nat. Photonics* (2010), 4, 611–622; (doi:10.1038/nphoton.2010.186).
- [8] D. S. Hecht, L. Hu, G. Irvin, Emerging transparent electrodes based on thin films of carbon nanotubes, graphene, metallic nanostructures, *Adv. Mater.* (2011), 23, 1482–1513; (doi:10.1002/adma.201003188).
- [9] Y. Li, Y. Chen, M. Qiu, H. Yu, X. Zhang, X. W. Sun, R. Chen, Preparation of Aluminum Nanomesh Thin Films from an Anodic Aluminum Oxide Template as Transparent Conductive Electrodes, *Scientific Reports* (2016), 6, 20114; (doi:10.1038/srep20114).
- [10] F. Lacy, Developing a theoretical relationship between electrical resistivity, temperature, film thickness for conductors, *Nanoscale Res. Lett.* (2011), 6, 636; (doi:10.1186/1556-276X-6-636).
- [11] A. Dhar, T. L. Alford, High quality transparent  $\text{TiO}_2/\text{Ag}/\text{TiO}_2$  composite electrode films deposited on flexible substrate at room temperature by sputtering, *APL Mater.* (2013), 1, 12102; (doi:10.1063/1.4808438).
- [12] J. Yan, X. Sun, Y. Zhu, Y. Zhao,  $\text{ZnO}/\text{Ag}/\text{ZnO}$  multilayer films deposited at room temperature, *Proc. of SPIE* (2008), 6624, 662413; (doi:10.1117/12.791110).
- [13] Q. Zhou, Z. Ji, B. Hu, C. Chen, L. Zhao, C. Wang, Low resistivity transparent conducting  $\text{CdO}$  thin films deposited by DC reactive magnetron sputtering at room temperature, *Mater. Lett.* (2007), 61, 531–534; (doi:10.1016/j.matlet.2006.05.004).
- [14] M. Kul, A. S. Aybek, E. Turan, M. Zor, S. Irmak, Effects of fluorine doping on the structural properties of the  $\text{CdO}$  films deposited by ultrasonic spray pyrolysis, *Sol. Energ. Mat. Sol. C.* (2007), 91, 1927–1933; (doi:10.1016/j.solmat.2007.07.014).
- [15] Z. Zhao, D.L. Morel, C.S. Ferekides, Electrical and optical properties of tin-doped  $\text{CdO}$  films deposited by atmospheric metalorganic chemical vapor deposition, *Thin Solid Films* (2002), 413, 203–211; (doi:10.1016/S0040-6090(02)00344-9).
- [16] C. G. Elinder, HEALTH HAZARDS FROM ENVIRONMENTAL OR OCCUPATIONAL EXPOSURE TO CADMIUM, *Acta Pharmacol. Toxl.* (1986), 59, 24–30; (doi:10.1111/j.1600-0773.1986.tb02700.x).
- [17] C. G. Granqvist, A. Hultåker, Transparent and conducting ITO films: new developments and applications, *Thin Solid Films* (2002), 411, 1–5; (doi:10.1016/S0040-6090(02)00163-3).

- [18] N. Al-Dahoudi, M. A. Aegerter, Comparative study of transparent conductive  $\text{In}_2\text{O}_3:\text{Sn}$  (ITO) coatings made using a sol and a nanoparticle suspension, *Thin Solid Films* (2006), 502, 193–197; (doi:10.1016/j.tsf.2005.07.273).
- [19] H. Cho, Y.-H. Yun, Characterization of indium tin oxide (ITO) thin films prepared by a sol–gel spin coating process, *Ceram. Int.* (2011), 37, 615–619; (doi:10.1016/j.ceramint.2010.09.033).
- [20] H. Y. Valencia, L. C. Moreno, A. M. Ardila, Structural, electrical and optical analysis of ITO thin films prepared by sol–gel, *Microelectr. J.* (2008), 39, 1356–1357; (doi:10.1016/j.mejo.2008.01.036).
- [21] T. Minami, Present status of transparent conducting oxide thin-film development for Indium-Tin-Oxide (ITO) substitutes, *Thin Solid Films* (2008), 516, 5822–5828; (doi:10.1016/j.tsf.2007.10.063).
- [22] A. V. Moholkar, S. M. Pawar, K. Y. Rajpure, C. H. Bhosale, J. H. Kim, Effect of fluorine doping on highly transparent conductive spray deposited nanocrystalline tin oxide thin films, *Appl. Surf. Sci.* (2009), 255, 9358–9364; (doi:10.1016/j.apsusc.2009.07.035).
- [23] Nanocs Inc., Online: <http://www.nanocs.com/ITO.htm>; last accessed 2017\_05\_20.
- [24] A. Janotti, C. G. Van de Walle, Fundamentals of zinc oxide as a semiconductor, *Rep. Prog. Phys.* (2009), 72, 126501; (doi:10.1088/0034-4885/72/12/126501).
- [25] Z.-N. Ng, K.-Y. Chan, C.-Y. Low, S. A. Kamaruddin, M. Z. Sahdan, Al and Ga doped ZnO films prepared by a sol–gel spin coating technique, *Ceram. Int.* (2015), 41, S254–S258; (doi:10.1016/j.ceramint.2015.03.183).
- [26] C.-Y. Chen, L.-H. Hsiao, J.-I. Chyi, Low resistivity and low compensation ratio Ga-doped ZnO films grown by plasma-assisted molecular beam epitaxy, *J. Cryst. Growth* (2015), 425, 216–220; (doi:10.1016/j.jcrysgro.2015.02.034).
- [27] T. Shirahata, T. Kawaharamura, S. Fujita, H. Orita, Transparent conductive zinc-oxide-based films grown at low temperature by mist chemical vapor deposition, *Thin Solid Films* (2015), 597, 30–38; (doi:10.1016/j.tsf.2015.11.006).
- [28] B. P. Shantheyanda, V. O. Todi, K. B. Sundaram, A. Vijayakumar, I. Oladeji, Compositional study of vacuum annealed Al doped ZnO thin films obtained by RF magnetron sputtering, *J. Vac. Sci. Technol. A.* (2011), 29, 51514; (doi:10.1116/1.3624787).
- [29] D. McCoul, W. Hu, M. Gao, V. Mehta, Q. Pei, Recent Advances in Stretchable and Transparent Electronic Materials, *Adv. Electron. Mater.* (2016), 2, 1500407; (doi:10.1002/aelm.201500407).
- [30] M. J. Alam, D. C. Cameron, Preparation and properties of transparent conductive aluminum-doped zinc oxide thin films by sol–gel process, *J. Vac. Sci. Technol. A.* (2001), 19, 1642–1649; (doi:10.1116/1.1340659).
- [31] Y.-S. Ho, Y.-S. Chen, C.-H. Wu, Effect of Annealing Ambient on the Electrical and Optical Properties of Aluminum-Doped ZnO Films Produced via a Sol–Gel Process, *J. Electron. Mater.* (2014), 43, 2644–2650; (doi:10.1007/s11664-014-3114-5).
- [32] M. Gao, X. Wu, J. Liu, W. Liu, The effect of heating rate on the structural and electrical properties of sol–gel derived Al-doped ZnO films, *Appl. Surf. Sci.* (2011), 257, 6919–6922; (doi:10.1016/j.apsusc.2011.03.031).
- [33] B. B. Пасынков, B. C. Сорокин, *Материалы электронной техники*. Лань (2004).
- [34] H. Wang, M. Xu, J. Xu, M. Ren, L. Yang, Low temperature synthesis of sol–gel derived Al-doped ZnO thin films with rapid thermal annealing process, *J. Mater. Sci: Mater. Electron.* (2010), 21, 589–594; (doi:10.1007/s10854-009-9962-8).

- [35] K. Ellmer, R. Mientus, Carrier transport in polycrystalline transparent conductive oxides: A comparative study of zinc oxide and indium oxide, *Thin Solid Films* (2008), 516, 4620–4627; (doi:10.1016/j.tsf.2007.05.084).
- [36] Z. L. Pei, C. Sun, M. H. Tan, J. Q. Xiao, D. H. Guan, R. F. Huang, L. S. Wen, Optical and electrical properties of direct-current magnetron sputtered ZnO:Al films, *J. Appl. Phys.* (2001), 90, 3432–3436; (doi:10.1063/1.1398070).
- [37] K. Ellmer, Resistivity of polycrystalline zinc oxide films: current status and physical limit, *J. Phys. D: Appl. Phys.* (2001), 34, 3097–3108; (doi:10.1088/0022-3727/34/21/301).
- [38] D. K. Schroder, *Semiconductor Material and Device Characterization*, John Wiley & Sons, Inc. (2006); (doi:10.1002/0471749095).
- [39] F. M. Smits, Measurements of Sheet Resistivity with the Four-Point Probe, *Bell Syst Tech J* (1958), 37, 711–718; (doi:10.1002/j.1538-7305.1958.tb03883.x).
- [40] J. García-Martín, J. Gómez-Gil, E. Vázquez-Sánchez, Non-Destructive Techniques Based on Eddy Current Testing, *Sensors* (2011), 11, 2525–2565; (doi:10.3390/s110302525).
- [41] SURAGUS GmbH, Online: <https://www.suragus.com/en/applications/thin-film-characterization>; last accessed 2017\_05\_20.
- [42] L. Castañeda, Present Status of the Development and Application of Transparent Conductors Oxide Thin Solid Films, *Materials Sciences and Applications* (2011), 2, 1233–1242; (doi:10.4236/msa.2011.29167).
- [43] S. Shirakata, T. Sakemi, K. Awai, T. Yamamoto, Electrical and optical properties of large area Ga-doped ZnO thin films prepared by reactive plasma deposition, *Superlattice Microst.* (2006), 39, 218–228; (doi:10.1016/j.spmi.2005.08.045).
- [44] A. Prodi-Schwab, T. Lütthge, R. Jahn, B. Herbig, P. Löbmann, Modified procedure for the sol–gel processing of indium–tin oxide (ITO) films, *J. Sol-Gel Sci. Technol.* (2008), 47, 68–73; (doi:10.1007/s10971-008-1749-5).
- [45] Z. R. Khan, M. S. Khan, M. Zulfequar, M. Shahid Khan, Optical and Structural Properties of ZnO Thin Films Fabricated by Sol-Gel Method, *Materials Sciences and Applications* (2011), 2, 340–345; (doi:10.4236/msa.2011.25044).
- [46] M. H. Huang, S. Mao, H. Feick, H. Yan, Y. Wu, H. Kind, E. Weber, R. Russo, P. Yang, Room-Temperature Ultraviolet Nanowire Nanolasers, *Science* (2001), 292, 1897–1899; (doi:10.1126/science.1060367).
- [47] N. R. Jungwirth, Y. Y. Pai, H. S. Chang, E. R. MacQuarrie, K. X. Nguyen, G. D. Fuchs, A single-molecule approach to ZnO defect studies: Single photons and single defects, *J. Appl. Phys.* (2014), 116, 043509; (doi:10.1063/1.4890979).
- [48] A. Loot, L. Dolgov, S. Pikker, R. Löhmus, I. Sildos, *Goniometric Setup for Plasmonic Measurements and Characterization of Optical Coatings*, in *Nanomaterials Imaging Techniques, Surface Studies, and Applications*, Springer Proc. Phys. (2013), 146, 119–134; (doi:10.1007/978-1-4614-7675-7\_10).
- [49] W. L. Barnes, Surface plasmon–polariton length scales: a route to sub-wavelength optics, *J. Opt. A: Pure Appl. Opt.* (2006), 8, S87–S93; (doi:10.1088/1464-4258/8/4/S06).
- [50] R. Sainidou, J. Renger, T. V. Teperik, M. U. González, R. Quidant, F. J. García de Abajo, Extraordinary All-Dielectric Light Enhancement over Large Volumes, *Nano Lett.* (2010), 10, 4450–4455; (doi:10.1021/nl102270p).
- [51] A. Polman, H. A. Atwater, Photonic design principles for ultrahigh-efficiency photovoltaics, *Nat. Mater.* (2012), 11, 174–177; (doi:10.1038/nmat3263).



- [52] T. Bora, H. H. Kyaw, J. Dutta, Plasmon Resonance Enhanced Zinc Oxide Photoelectrodes for Improvement in Performance of Dye Sensitized Solar Cells, *Mater. Sci. Forum* (2014), 771, 91–101; (doi:10.4028/www.scientific.net/MSF.771.91).
- [53] H. Raether, *Surface Plasmons on Smooth and Rough Surfaces and on Gratings*, Springer-Verlag (1988).
- [54] J. R. Sambles, G. W. Bradbery, F. Yang, Optical excitation of surface plasmons: An introduction, *Contemp. Phys.* (1991), 32, 173–183; (doi:10.1080/00107519108211048).
- [55] S. D. Choudhury, R. Badugu, K. Ray, J. R. Lakowicz, Steering Fluorescence Emission with Metal-Dielectric-Metal Structures of Au, Ag, Al, *J. Phys. Chem. C* (2013), 117, 15798–15807; (doi:10.1021/jp4051066).
- [56] J. S. Yuk, C. McDonagh, B. D. MacCraith, Demonstration of a surface plasmon-coupled emission (SPCE)-based immunoassay in the absence of a spacer layer, *Anal. Bioanal. Chem.* (2010), 398, 1947–1954; (doi:10.1007/s00216-010-4026-8).
- [57] J. Seidel, S. Grafström, L. Eng, Stimulated Emission of Surface Plasmons at the Interface between a Silver Film and an Optically Pumped Dye Solution, *Phys. Rev. Lett.* (2005), 94, 177401; (doi:10.1103/PhysRevLett.94.177401).
- [58] M. A. Noginov, G. Zhu, M. Mayy, B. A. Ritzo, N. Noginova, V. A. Podolskiy, Stimulated Emission of Surface Plasmon Polaritons, *Phys. Rev. Lett.* (2008), 101, 226806; (doi:10.1103/PhysRevLett.101.226806).
- [59] M. Čepič, Liquid Crystals in Education – The Basics, *European J. of Physics Education*. (2012), 4, 27–33.
- [60] C. Gu, P. Yeh, *Liquid Crystal Display (LCD)*, in *Handbook of Digital Imaging*, John Wiley & Sons, Ltd (2015); (doi:10.1002/9781118798706.hdi018).
- [61] S. Shama, U. Jindal, M. Goyal, S. Sharma, V. Goyal, A Review- on Different Types of Displays, *International Journal of Multimedia and Ubiquitous Engineering* (2016), 11, 327–332; (doi:10.14257/ijmue.2016.11.8.33).
- [62] P. F. Bai, R. A. Hayes, M. L. Jin, L. L. Shui, Z. C. Yi, L. Wang, X. Zhang, G. F. Zhou, Review of Paper-Like Display Technologies, *Progress In Electromagnetics Research* (2014), 147, 95–116; (doi:10.2528/PIER13120405).
- [63] J. Hoogboom, T. Rasing, A. E. Rowan, R. J. M. Nolte, LCD alignment layers. Controlling nematic domain properties, *J. Mater. Chem.* (2006), 16, 1305–1314; (doi:10.1039/B510579J).
- [64] B.-Y. Oh, M.-C. Jeong, T.-H. Moon, W. Lee, J.-M. Myoung, J.-Y. Hwang, D.-S. Seo, Transparent conductive Al-doped ZnO films for liquid crystal displays, *J. Appl. Phys.* (2006), 99, 124505; (doi:10.1063/1.2206417).
- [65] Y. U. Jung, K.-W. Park, S.-T. Hur, S.-W. Choi, S. J. Kang, High-transmittance liquid-crystal displays using graphene conducting layers, *Liq. Cryst.* (2014), 41, 101–105; (doi:10.1080/02678292.2013.837517).
- [66] O. Tuna, Y. Selamet, G. Aygun, L. Ozyuzer, High quality ITO thin films grown by dc and RF sputtering without oxygen, *J. Phys. D: Appl. Phys.* (2010), 43, 55402; (doi:10.1088/0022-3727/43/5/055402).
- [67] R. Pandey, S. Yuldashev, H. D. Nguyen, H. C. Jeon, T. W. Kang, Fabrication of aluminium doped zinc oxide (AZO) transparent conductive oxide by ultrasonic spray pyrolysis, *Curr. Appl. Phys.* (2012), 12, S56–S58; (doi:10.1016/j.cap.2012.05.027).
- [68] W.-J. Chen, W.-L. Liu, S.-H. Hsieh, Y.-G. Hsu, Synthesis of ZnO:Al Transparent Conductive Thin Films Using Sol-gel Method, *Procedia Engineer.* (2012), 36, 54–61; (doi:10.1016/j.proeng.2012.03.010).

- [69] C. Brinker, G. W. Scherer, *Sol - gel science*, Academic Press, Inc.(1990).
- [70] L. Znaidi, Sol-gel-deposited ZnO thin films: A review, *Materials Science and Engineering: B* (2010), 174, 18–30; (doi:10.1016/j.mseb.2010.07.001).
- [71] G. Taylor, Electrically Driven Jets, *Proceedings of the Royal Society A* (1969), 313, 453–475; (doi:10.1098/rspa.1969.0205).
- [72] A. K. Haghi, M. Akbari, Trends in electrospinning of natural nanofibers, *Phys. Stat. sol.* (2007), 204, 1830–1834; (doi:10.1002/pssa.200675301).
- [73] J. Deitzel, J. Kleinmeyer, D. Harris, N. C. Beck Tan, The effect of processing variables on the morphology of electrospun nanofibers and textiles, *Polymer* (2001), 42, 261–272; (doi:10.1016/S0032-3861(00)00250-0).
- [74] M. M. Hohman, M. Shin, G. Rutledge, M. P. Brenner, Electrospinning and electrically forced jets. II. Applications, *Physics of Fluids* (2001), 13, 2221; (doi:10.1063/1.1384013).
- [75] W. Zuo, M. Zhu, W. Yang, H. Yu, Y. Chen, Y. Zhang, Experimental study on relationship between jet instability and formation of beaded fibers during electrospinning, *Polym. Eng. Sci.* (2005), 45, 704–709; (doi:10.1002/pen.20304).
- [76] C. Zhang, X. Yuan, L. Wu, Y. Han, J. Sheng, Study on morphology of electrospun poly(vinyl alcohol) mats, *Eur. Polym. J.* (2005), 41, 423–432; (doi:10.1016/j.eurpolymj.2004.10.027).
- [77] X. Yuan, Y. Zhang, C. Dong, J. Sheng, Morphology of ultrafine polysulfone fibers prepared by electrospinning, *Polym. Int.* (2004), 53, 1704–1710; (doi:10.1002/pi.1538).
- [78] B. Sundaray, V. Subramanian, T. S. Natarajan, R.-Z. Xiang, C.-C. Chang, W.-S. Fann, Electrospinning of continuous aligned polymer fibers, *Appl. Phys. Lett.* (2004), 84, 1222; (doi:10.1063/1.1647685).
- [79] D. Li, Y. Wang, Y. Xia, Electrospinning Nanofibers as Uniaxially Aligned Arrays and Layer-by-Layer Stacked Films, *Adv. Mater.* (2004), 16, 361–366; (doi:10.1002/adma.200306226).
- [80] X. Wang, I. C. Um, D. Fang, A. Okamoto, B. S. Hsiao, B. Chu, Formation of water-resistant hyaluronic acid nanofibers by blowing-assisted electro-spinning and non-toxic post treatments, *Polymer* (2005), 46, 4853–4867; (doi:10.1016/j.polymer.2005.03.058).
- [81] C. S. Ki, D. H. Baek, K. D. Gang, K. H. Lee, I. C. Um, Y. H. Park, Characterization of gelatin nanofiber prepared from gelatin-formic acid solution, *Polymer* (2005), 46, 5094–5102; (doi:10.1016/j.polymer.2005.04.040).
- [82] C. L. Casper, J. S. Stephens, N. G. Tassi, D. B. Chase, J. F. Rabolt, Controlling Surface Morphology of Electrospun Polystyrene Fibers: Effect of Humidity and Molecular Weight in the Electrospinning Process, *Macromolecules* (2004), 37, 573–578; (doi:10.1021/ma0351975).
- [83] C. Mit-uppatham, M. Nithitanakul, P. Supaphol, Ultrafine Electrospun Polyamide-6 Fibers: Effect of Solution Conditions on Morphology and Average Fiber Diameter, *Macromol. Chem. Phys.* (2004), 205, 2327–2338; (doi:10.1002/macp.200400225).
- [84] E. Kretschmann, H. Raether, Notizen: Radiative Decay of Non Radiative Surface Plasmons Excited by Light, *Zeitschrift für Naturforsch. A* (1968), 23, 2135–2136; (doi:10.1515/zna-1968-1247).
- [85] M. L. Brongersma, P. G. Kik, *Surface Plasmon Nanophotonics*, Springer (2007), 131; (doi:10.1007/978-1-4020-4333-8).

- [86] Sigma-Aldrich Co. LLC., Online: <http://www.sigmaaldrich.com/catalog/product/sigma/64719?lang=en&region=EE>; last accessed 2017\_05\_20.
- [87] AppliChem GmbH, Online: <https://www.applichem.com/en/shop/product-detail/as/ethanol-99-vergaellt-mit-1-mek-zur-analyse>; last accessed 2017\_05\_20.
- [88] V. Musat, B. Teixeira, E. Fortunato, R. C. C. Monteiro, P. Vilarinho, Al-doped ZnO thin films by sol-gel method, *Surface and Coatings Technology* (2004), 180–181, 659–662; (doi:10.1016/j.surfcoat.2003.10.112).
- [89] S.-S. Kim, S.-Y. Choi, C. -G. Park, H.-W. Jin, Transparent conductive ITO thin films through the sol-gel process using metal salts, *Thin Solid Films* (1999), 347, 155–160; (doi:10.1016/S0040-6090(98)01748-9).
- [90] M. S. Kim, K. G. Yim, J.-S. Son, J.-Y. Leem, Effects of Al Concentration on Structural and Optical Properties of Al-doped ZnO Thin Films, *Bull. Korean Chem. Soc.* (2012), 33, 1235–1241; (doi:10.5012/bkcs.2012.33.4.1235).
- [91] G. J. Exarhos, X.-D. Zhou, Discovery-based design of transparent conducting oxide films, *Thin Solid Films* (2007), 515, 7025–7052; (doi:10.1016/j.tsf.2007.03.014).
- [92] B. Ding, T. Ogawa, J. Kim, K. Fujimoto, S. Shiratori, Fabrication of a super-hydrophobic nanofibrous zinc oxide film surface by electrospinning, *Thin Solid Films* (2008), 516, 2495–2501; (doi:10.1016/j.tsf.2007.04.086).
- [93] J. Kim, S. Yoon, J.-K. Yoo, J. Kim, H. Kim, K. Kang, Highly Laminated Electrospun ZnO Nanofibrous Film on the Transparent Conducting Oxide for Photovoltaic Device, *J. Electrochem. Sci. Te.* (2012), 3, 68–71; (doi:10.5229/JECST.2012.3.2.68).
- [94] S. Yun, S. Lim, Effect of Al-doping on the structure and optical properties of electrospun zinc oxide nanofiber films, *J. Colloid Interf. Science* (2011), 360, 430–439; (doi:10.1016/j.jcis.2011.05.022).
- [95] S. K. Nataraj, B. H. Kim, J. H. Yun, D. H. Lee, T. M. Aminabhavi, K. S. Yang, Electrospun Nanocomposite Fiber Mats of Zinc-Oxide Loaded Polyacrylonitrile, *Carbon letters* (2008), 9, 108–114; (doi:10.5714/CL.2008.9.2.108).
- [96] B. Zhou, Y. Wu, L. Wu, K. Zou, H. Gai, Effects of Al dopants on the microstructures and optical properties of ZnO nanofibers prepared by electrospinning, *Physica E: Low-dimensional Systems and Nanostructures* (2009), 41, 705–710; (doi:10.1016/j.physe.2008.11.017).
- [97] C. Jang, S. M. Lee, K. C. Choi, Optical characteristics of  $\text{YVO}_4\text{:Eu}^{3+}$  phosphor in close proximity to Ag nanofilm: emitting layer for mirror-type displays, *Optics Express* (2012), 20, 2143; (doi:10.1364/OE.20.002143).
- [98] D. Y. Lei, C. Ong, Enhanced forward emission from ZnO via surface plasmons, *Appl. Phys. Lett.* (2007), 91, 211107; (doi:10.1063/1.2805022).
- [99] K. Aslan, M. J. R. Previte, Y. Zhang, C. D. Geddes, Metal-Enhanced Fluorescence from Nanoparticulate Zinc Films, *J. Phys. Chem. C* (2008), 112, 18368–18375; (doi:10.1021/jp806790u).
- [100] J. S. Yuk, M. Trnavsky, C. McDonagh, B. D. MacCraith, Surface plasmon-coupled emission (SPCE)-based immunoassay using a novel paraboloid array biochip, *Biosens. Bioelectron.* (2010), 25, 1344–1349; (doi:10.1016/j.bios.2009.10.026).
- [101] Z. Dong, B. Han, S. Qian, D. Chen, Fluorescent Properties of ZnO Nanostructures Fabricated by Hydrothermal Method, *J. Nanomater.* (2012), 2012, pp. 1–5; (doi:10.1155/2012/251276).

- [102] H.-G. Unger, *Planar optical waveguides and fiber*, Oxford University Press (1977).
- [103] W. N. Hansen, Electric Fields Produced by the Propagation of Plane Coherent Electromagnetic Radiation in a Stratified Medium, *J. Opt. Soc. Am.* (1968), 58, 380-390; (doi:10.1364/JOSA.58.000380).
- [104] F. Abelès, Optical Properties of Thin Absorbing Films, *J. Opt. Soc. Am.* (1957), 47, 473-482; (doi:10.1364/JOSA.47.000473).
- [105] J. Chilwell, I. Hodgkinson, Thin-films field-transfer matrix theory of planar multilayer waveguides and reflection from prism-loaded waveguides, *J. Opt. Soc. Am. A* (1984), 1, 742-753; (doi:10.1364/JOSAA.1.000742).
- [106] R. F. Oulton, V. J. Sorger, D. A. Genov, D. F. P. Pile, X. Zhang, A hybrid plasmonic waveguide for subwavelength confinement and long-range propagation, *Nat. Photonics* (2008), 2, 496–500; (doi:10.1038/nphoton.2008.131).
- [107] J. GRANDIDIER, G. C. DES FRANCS, S. MASSENOT, A. BOUHELIER, L. MARKEY, J.-C. WEEBER, A. DEREUX, Leakage radiation microscopy of surface plasmon coupled emission: investigation of gain-assisted propagation in an integrated plasmonic waveguide, *Journal of Microscopy* (2010), 239, 167-172; (doi:10.1111/j.1365-2818.2010.03368.x).
- [108] L. Dolgov, V. Kiisk, R. Matt, S. Pikker, I. Sildos, Tailoring of the spectral–directional characteristics of rare-earth fluorescence by metal–dielectric planar structures, *Appl. Phys. B* (2012), 107, 749–753; (doi:10.1007/s00340-012-5025-6).
- [109] V. Boiko, G. Dovbeshko, L. Dolgov, V. Kiisk, I. Sildos, A. Loot, V. Gorelik, Angular shaping of fluorescence from synthetic opal-based photonic crystal, *Nanoscale Res. Lett.* (2015), 10, 97; (doi:10.1186/s11671-015-0781-y).
- [110] F. Haraguchi, K. Inoue, N. Toshima, S. Kobayashi, K. Takatoh, Reduction of the Threshold Voltages of Nematic Liquid Crystal Electrooptical Devices by Doping Inorganic Nanoparticles, *Jpn. J. Appl. Phys.* (2007), 46, L796–L797; (doi:10.1143/JJAP.46.L796).

## **PUBLICATIONS**

## CURRICULUM VITAE

**Name:** Vladimir Ivanovich Kondratiev  
**Date of birth:** October 4, 1986  
**Nationality:** Russian  
**Phone number:** +372 5816 9703  
**E-mail:** kondraty@ut.ee

### Education:

2011–present University of Tartu, Department of Materials Science, PhD student  
2008–2010 Saint Petersburg State Electrotechnical University “LETI”, Department of Microelectronics, Saint Petersburg, Russia. M.Sc. Engineering and Technologies. Specialization: Nanotechnology and Diagnostics.  
2004–2008 Saint Petersburg State Electrotechnical University “LETI”, Department of Microelectronics, Saint Petersburg, Russia. B.Sc. Engineering and Technologies.  
1993–2004 Gatchina Lyceum #3, Leningrad Oblast, Russia.

**Languages:** Russian (native), English (sufficient), Estonian (basic).

### Career:

2010–2011 Engineer “NT-SPb”. Responsibilities: AFM research, AFM technical support, company representative at exhibitions.  
2007–2010 Laboratory of nanoelectronics, St. Petersburg State Electrotechnical University “LETI”. Responsibilities: Capacitance spectroscopy research.

### Publications included in the thesis:

- I. V.I. Kondratiev, I. Kink, A.E. Romanov, LOW TEMPERATURE SOL-GEL TECHNIQUE FOR PROCESSING AL-DOPED ZINC OXIDE FILMS, Materials Physics and Mechanics (2013), 17, 38–46.
- II. V.I. Kondratiev, I. Kink, A.E. Romanov, L. Dolgov, TRANSPARENT FILMS FROM ALUMINIUM-DOPED ZINC OXIDE FIBERS PREPARED BY ELECTROSPINNING METHOD, Materials Physics and Mechanics (2016), 27, 133–141.
- III. L. Dolgov, V.I. Kondratiev, A. Loot, V. Kiisk, S. Lange, Resonant control of fluorescence from aluminium doped zinc oxide films, Optical and Quantum Electronics (2016), 48, 522; (doi:10.1007/s11082-016-0794-5).

**Other publications:**

- IV. L. Dolgov, O. Fesenko, V. Kavelin, O. Budnyk, V. Estrela-Llopis, A. Chevychalova, T. Repän, V.I. Kondratiev, S. Mamykin, Gold micro- and nano-particles for surface enhanced vibrational spectroscopy of pyridostigmine bromide, *Vibrational Spectroscopy* (2017), 88, 71–79; (doi:10.1016/j.vibspec.2016.11.005).

**Scholarships and honor:**

- 2016–present** PhD scholarship, University of Tartu.  
Aug.2016 Archimedes foundation DoRa scholarship for short time foreign conference visit, Department of Materials Science, University of Tartu  
2011–2015 Archimedes foundation DoRa scholarship for full time PhD student – Department of Materials Science, University of Tartu  
2010 Graduated with a medal 'For the best research student work'. All-Russian universities students research works competition in the field of nanotechnology and nanomaterials.  
<http://www.saint.mephi.ru>

**Other research related contribution (presentations at conferences/symposiums):**

- 24–27 August, 2016, Lviv, Ukraine 4th International research and practice conference “Nanotechnology and nanomaterials nano-2016”. Directional resonance fluorescence from the ZnO:Al films (oral presentation).  
26–29 April, 2016, St. Petersburg, Russia 5th International Scientific Conference State-of-the-art Trends of Scientific Research of Artificial and Natural Nanoobjects "STRANN 2016. Electrospinning method for preparation fiber based al-doped zinc oxide films (oral presentation).  
28–30 March, 2016, St. Petersburg, Russia 3rd International School and Conference on Optoelectronics, Photonics, Engineering and Nanostructures “Saint Petersburg OPEN 2016”. Preparation fiber based al-doped zinc oxide films by electrospinning method (poster presentation).  
21–24 April, 2013, Tartu, Estonia Functional Materials and Nanotechnologies. Sol-gel technics for processing transparent and conductive Al-doped zinc oxide films (poster presentation).  
07–08 March, 2013, Tallinn, Estonia TÜ ja TTÜ doktorikooli “Funktsionaalsed materjalid ja tehnoloogiad” esimene teaduskonverents. Optimization of sol-gel techniques for fabrication of transparent and conductive Al-doped Zinc Oxide films (poster presentation).

- Hobbies:** Travelling, information technology, microelectronics.

## ELULOOKIRJELDUS

**Name: Nimi:** Vladimir Ivanovich Kondratiev  
**Sünniaeg:** 4. oktoober, 1986  
**Kodakondsus:** Venemaa  
**Telefon:** +372 5816 9703  
**E-post:** kondraty@ut.ee

### Haridustee:

2011– praegusel ajal Tartu Ülikool, Materjaliteaduse osakond, materjali-  
teaduse doktorant  
2008–2010 St. Peterburi Riiklik Elektrotehnika Ülikool “LETI”,  
Mikroelektroonika osakond, St. Peterburi, Venemaa.  
Omandatud magistrikraad tehnikateadustes (eriala:  
nanotehnoloogia ja diagnostika).  
2004–2008 St. Peterburi Riiklik Elektrotehnika Ülikool “LETI”,  
Mikroelektroonika osakond, St. Peterburi, Venemaa.  
Omandatud bakalaureuse kraad tehnikateadustes.  
1993–2004 Gatšina Lütseum #3, Leningradi oblast, Venemaa.

### Keelteoskus:

Vene (emakeel), English (piisav), Estonian (elementaarne).

### Career:

2010–2011 Insener “NT-SPb”. Vastutused: AFM uurimistöö,  
AFM tehniline abi, firma esindaja näitustel.  
2007–2010 Nanoelektroonika labor, St. Peterburi Riiklik Elektro-  
tehnika Ülikool “LETI”. Vastutused: Mahtuvuse  
spektroskoopia uurimistöö.

### Põhipublikatsioonid doktoritöös:

- I. V.I. Kondratiev, I. Kink, A.E. Romanov, LOW TEMPERATURE SOL-  
GEL TECHNIQUE FOR PROCESSING AL-DOPED ZINC OXIDE  
FILMS, Materials Physics and Mechanics (2013), 17, 38–46.
- II. V.I. Kondratiev, I. Kink, A.E. Romanov, L. Dolgov, TRANSPARENT  
FILMS FROM ALUMINIUM-DOPED ZINC OXIDE FIBERS  
PREPARED BY ELECTROSPINNING METHOD, Materials Physics  
and Mechanics (2016), 27, 133–141.
- III. L. Dolgov, V.I. Kondratiev, A. Loot, V. Kiisk, S. Lange, Resonant  
control of fluorescence from aluminium doped zinc oxide films, Optical  
and Quantum Electronics (2016), 48, 522; (doi:10.1007/s11082-016-  
0794-5).



**Publikatsioonid, mis ei ole doktoritööga seotud:**

- IV. L. Dolgov, O. Fesenko, V. Kavelin, O. Budnyk, V. Estrela-Llopis, A. Chevychalova, T. Repän, V.I. Kondratiev, S. Mamykin, Gold micro- and nano-particles for surface enhanced vibrational spectroscopy of pyridostigmine bromide, *Vibrational Spectroscopy* (2017), 88, 71–79; (doi:10.1016/j.vibspec.2016.11.005).

**Saadud uurimistoetused ja autasud:**

- 2016–praegusel ajal  
Aug.2016 Doktorandi stipendium, Tartu Ülikool.  
DoRa stipendium (Eesti Hariduse ja Teaduse Heaks, Archimedes) lühiajaliseks viibimiseks välismaal konverentsil, Materjaliteaduse osakond, Tartu Ülikool
- 2011–2015 DoRa täiskohaga doktorandistipendium (Eesti Hariduse ja Teaduse Heaks, Archimedes), Materjaliteaduse osakond, Tartu Ülikool
- 2010 Lõpetanud medaliga “Parima üliõpilase uurimistöö eest”. Ülevenemaaline üliõpilaste uurimistööde võistlus valdkonnas “Nanotehnoloogia ja nanomaterjalid”.  
<http://www.saint.mephi.ru>

**Teised teadustööga seotud tegevused (konverentside ettekanded):**

- 24–27 August, 2016, Lviv, Ukraine 4th International research and practice conference “Nanotechnology and nanomaterials nano-2016”. Directional resonance fluorescence from the ZnO:Al films (oral presentation).
- 26–29 April, 2016, St. Petersburg, Russia 5th International Scientific Conference State-of-the-art Trends of Scientific Research of Artificial and Natural Nanoobjects “STRANN 2016”. Electrospinning method for preparation fiber based al-doped zinc oxide films (oral presentation).
- 28–30 March, 2016, St. Petersburg, Russia 3rd International School and Conference on Optoelectronics, Photonics, Engineering and Nanostructures “Saint Petersburg OPEN 2016”. Preparation fiber based al-doped zinc oxide films by electrospinning method (poster presentation).
- 21–24 April, 2013, Tartu, Estonia Functional Materials and Nanotechnologies. Sol-gel technics for processing transparent and conductive Al-doped zinc oxide films (poster presentation).
- 07–08 March, 2013, Tallinn, Estonia TÜ ja TTÜ doktorikooli “Funktsionaalsed materjalid ja tehnoloogiad” esimene teaduskonverents. Optimization of sol-gel techniques for fabrication of transparent and conductive Al-doped Zinc Oxide films (poster presentation).

**Huvialad:**

Reisimine, infotehnoloogia, mikroelektroonika.

## DISSERTATIONES SCIENTIAE MATERIALIS UNIVERSITATIS TARTUENSIS

1. **Martin Järvekülg.** Tubular microstructures by Hf-, Zr- and Ti-butoxide gel sheet rolling. Tartu, 2011, 112 p.
2. **Sergei Vlassov.** Investigation of nanoscale interactions and mechanical properties of nanostructures using quartz tuning fork based real-time measurements. Tartu, 2011, 171 p.
3. **Margus Kodu.** Pulsed Laser Deposition of Magnesium Oxide and Barium Ternary Oxides for Plasma Display Protective Layers. Tartu, 2011, 89 p.
4. **Rainer Pärna.** Surface studies of some oxide films. Tartu, 2011, 129 p.
5. **Jevgeni Šulga.** Self-assembly and interaction of nanostructures. Tartu, 2011, 114 p.
6. **Wojciech Kuznik.** Quantum-chemical computer simulations of the linear and non-linear optical properties of pyrazoloquinoline and dicyanopyrazine derivatives. Tartu, 2012, 89 p.
7. **Leonid Dorogin.** Structural and tribological properties of zero- and one-dimensional nanocrystals. Tartu, 2012, 193 p.
8. **Viljar Palmre.** Fabrication and characterization of microporous carbon-based electroactive polymer actuators. Tartu, 2012, 99 p.
9. **Madis Paalo.** Synthesis of CNT-metal oxide nanocomposites: sol-gel process, rheology, structural and functional properties. Tartu, 2014, 175 p.
10. **Raul Välbe.** Development of ionic liquid composites by sol-gel method for elaboration of industrial nano- and microstructures. Tartu, 2014, 97 p.
11. **Urmas Joost.** Impurity and preparation dependent properties of titania thin films. Tartu, 2014, 155 p.
12. **Madis Umalas.** Application of sol-gel technology for production of ceramic nanocomposites and functional coatings. Tartu, 2015, 136 p.
13. **Elena Samsonova.** Energy transfer probe as a tool to study morphological and structural origins of fluorescence quenching in rare-earth doped nanophosphors. Tartu, 2015, 114 p.
14. **Jay Mondal.** Novel Corrosion Protective Nanostructured Composite Coatings. Tartu, 2016, 104 p.
15. **Kathriin Utt.** Metal oxide mesostructures for optical applications. Tartu, 2016, 88 p.
16. **Kaido Siimon.** Electrospun gelatin cross-linked by glucose. Tartu, 2016, 84 p.
17. **Marko Part.** Combined three-dimensional sol-gel structures and atomic layer deposited thin films. Tartu, 2017, 162 p.
18. **Pejman Rasti.** Analysis of Remote Sensing Image Super Resolution using Fluid Lenses. Tartu, 2017, 188 p.
19. **Ivo Romet.** Recombination luminescence of doped borates: origin and application prospects in dosimetry. Tartu, 2017, 111 p.